Engineering Fluid Dynamics

An experimental setup for validation of the plane wave methods.

Thesis Mechanical Engineering

UNIVERSITY OF TWENTE.

Author:
S.R.Liet

Student number:
s2191121

Supervisor:
Y.H.Wijnant

Graduation number
443

February 15, 2024

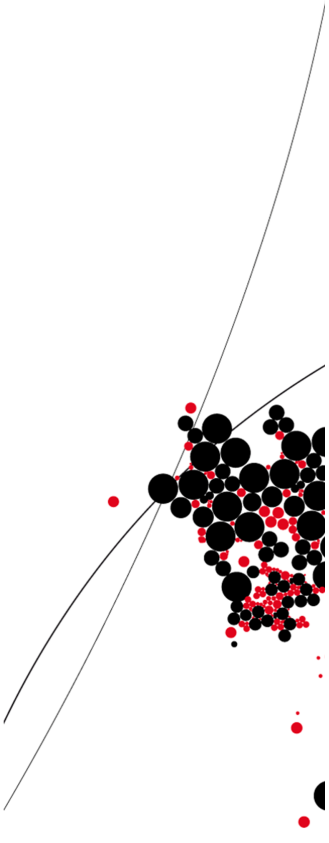

Table of Contents

1 Summary

In this paper, experiments are described which will serve to validate the, so called, plane wave decomposition(PWD); a method to measure in-situ absorption coefficients. A box (setup) has been build which consists of a cavity and a loudspeaker. The horizontal dimensions of the cavity can be altered, whereas, for simplicity, the height of the box has been designed to be sufficiently low. This is done to ensure a 2 dimensional sound field within the box. At various positions in the box, a number of closely spaced microphones have been used to measure the acoustic pressures within the cavity. Two methods have been implemented to derive the particle velocity from these measurements; one method is based on 2 microphones and one, a more accurate method, is based on 3 microphones. The results of the calculations of the experimental tests are compared with the results of the calculations of the simulated tests. These experimental and simulated results show similarities in absorption coefficient.

2 Introduction

In acoustic applications the sound absorption coefficient α is an important property. The absorption coefficient describes the percentage of the incoming sound energy being absorbed by a material, i.e. if all sound energy is absorbed by the material, the absorption coefficient is 1. If all sound energy is reflected, the absorption coefficient is -1, and if the sound energy is neither absorbed or reflected the absorption coefficient is 0. The value is important in room acoustics and general noise control for instance. The sound absorption coefficient α is known to be dependent on multiple factors and it is not only a material property. In previous studies it was shown that the, so-called, Local Plane Wave (LPW) method can be used to, in-situ, determine the sound absorption coefficient in simulations. The method is based on a local plane wave assumption, where the acoustic pressure and the component of the particle velocity in the direction of the absorber is used to approximate the incident and reflected sound intensity. With these approximated sound intensities the absorption coefficient can be calculated. The purpose of this thesis is to evaluate if the PWD method can be validated with the use of an experimental test setup, for simplicity in a 2D scenario.
Chapter 2 discusses a more accurate method, the so-called plane wave decomposition, as given in [1]. Although this improved method is more accurate and was shown to work in most parts of a simulated sound field, it did not work in some parts of the sound field and the results were not well understood.
In this research, we initiate the investigation of the methods experimentally. For this, we have developed a test box of which the height is sufficiently small to obtain a 2D sound field. A sound source is used to produce sound inside the box and multiple microphones are used to measure the pressure field and approximate the acoustic particle velocity near an absorber placed in the box.
Chapter 3 explains the configured test setup in detail. These details consist of the functioning of the experimental test setup, the choices of the equipment and materials used in the experimental test setup and transferring of the gathered measurements from the experimental test setup to usable data.
Chapter 4 explains the usage of the data (both simulated and experimental). The data of both the test setups, in the experimental test setup gained by the microphones, are realized by measurements, which is implemented in MATLAB. In this software program calculations are done by applying the LPW method on the microphones to calculate the Sound Power Level(L_p), Velocity Level(L_v) and the absorption coefficient. The calculations of the absorption coefficient are explained in this chapter, as the analyses regarding the L_p and the L_v are rather 'simple' compared to the analyses of the absorption coefficient.
Chapter 5 shows the results of the simulations and the experiments done. The results are explained in three subsections. In the first subsection the results are shown where an absorbing material is placed in the test setup where the measurements of the microphones are done at it's two extremes, farthest point away from the speaker and closest point from the speaker. In the second subsection, the results of the calculation of the absorption coefficient are shown for either two or three microphones, the differences are explained. In the third subsection, the results of the calculations are shown for different thicknesses of the absorbing material in the cavity. Also explanation is given of these results.
In Chapter 6 the conclusion and discussion are given about the research done.

3 Theory & Simulations

3.1 The Theory

Ysbrand Wijnant first initiated a research using a local plane wave assumption [2] to measure the effective in situ sound absorption coefficient[3]. The method introduced to estimate this absorption coefficient is called the LPW-Method. As the formula for the (average) absorption coefficient for a given sound field is:

$$\alpha = \frac{W_{ac}}{W_{in}}, \tag{1}$$

where W_{ac} is the active (net) acoustic power flowing through a surface and W_{in} is the power flowing through the same surface, if no reflection occurs. The W_{ac} and the W_{in} can be rewritten to:

$$W_{ac} = \int_S \mathbf{I_{ac}} \cdot \mathbf{n} dS; \quad W_{in} = \int_S \mathbf{I_{in}} \cdot \mathbf{n} dS \tag{2}$$

These incident and reflected intensity is illustrated in Figure 1

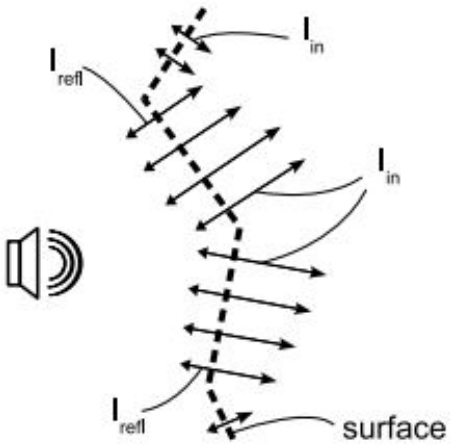

Figure 1: The incident and reflective intensity(taken from:[4])

As the active intensity can be calculated through the provided formula $\left(\mathbf{I_{ac}} \cdot \mathbf{n} = \frac{1}{2}\Re(P\bar{\mathbf{U}} \cdot \mathbf{n})\right)$, no specific formula is offered for the incident intensity I_{in}. However, by measuring the pressure and normal velocity in the vicinity of any given point the incident intensity can be estimated. Based on the LPW theory, stating in a point, specified by the spatial coordinate $\mathbf{r}$ the measured pressure $\mathrm{P}(\mathbf{r})$ and complex velocity $\mathbf{U(r)}$ in a given direction $\mathbf{n}$, is a result of two plane waves propagating in the given directions:

$$P(\mathbf{r}) = A(\mathbf{r})e^{-ikx} + B(\mathbf{r})e^{ikx}; \quad \mathbf{U}(\mathbf{r}) \cdot \mathbf{n} = \frac{1}{\rho c}\left(A(\mathbf{r})e^{-ikx} + B(\mathbf{r})e^{ikx}\right) \tag{3}$$

A and B are the complex amplitudes for the incident wave and the reflected wave, k respectively denotes the wave number and the constants ρ and c, the density and the speed of sound. Setting the point of consideration to x = 0, the equations can be rewritten in terms of the amplitudes A($\mathbf{r}$) and B($\mathbf{r}$):

$$A(\mathbf{r}) = \frac{P(\mathbf{r}) + \rho c \mathbf{U}(\mathbf{r}) \cdot \mathbf{n}}{2}; \quad B(\mathbf{r}) = \frac{P(\mathbf{r}) - \rho c \mathbf{U}(\mathbf{r}) \cdot \mathbf{n}}{2} \tag{4}$$

From which the intensity of the incident wave and the intensity of the reflected wave are:

$$I_{in} = \frac{A\bar{A}}{2\rho c}; \quad I_{refl} = \frac{B\bar{B}}{2\rho c} \tag{5}$$

Through a series of experiments, Erwin Kuipers identified a potential working method that could be applied. Subsequently, he delved into further research to develop a method (the LSPW method) that could establish a relationship between an incoming wave A, arriving in a point at an angle α, and the resulting outgoing wave B, departing from the same point at the angle α:

$$I_{in}(\mathbf{r}) = \frac{\mid A(\mathbf{r}) \mid^2}{2\rho_0 c_0} cos(\alpha); \quad I_{refl}(\mathbf{r}) = \frac{\mid B(\mathbf{r}) \mid^2}{2\rho_0 c_0} cos(\alpha) \tag{6}$$

When this is filled into the equation for the active intensity and also the equation for the velocity becomes(taken $Z_0 = \rho_0 c_0$):

$$I_{ac}(\mathbf{r}) = \frac{|A(\mathbf{r}) - B(\mathbf{r})|}{2Z_0} cos(\alpha) \tag{7}$$

$$U_n(\mathbf{r}) = \frac{cos(\alpha)}{Z_0} [A(\mathbf{r}) - B(\mathbf{r})] \tag{8}$$

This method is called the LSPW method.
Based on this assumption, R. Bontekoning [1] further developed of Ir. Kuipers research. His primary objective was to devise a solution for waves in which the angle of the incoming wave A at a given point differs from the angle of the outgoing wave B at the same point. The variables that are measured up to this point are the complex pressure P and the complex velocity $\mathbf{U}$. These variables are defined as:

$$P = A + B \quad , \quad U_x = \frac{1}{\rho c}\big(A \cdot cos(\alpha) - B \cdot cos(\beta)\big) \quad , \quad U_y = \frac{1}{\rho c}\big(A \cdot sin(\alpha) + B \cdot sin(\beta)\big) \tag{9}$$

In the research of R. Bontekoning the made development to the formula is done by addressing the employment of a coordinate transformation.

First the active intensity is related to the pressure and the velocity the reactive intensity is also related to the pressure and the velocity:

$$\mathbf{I_{ac}} = \frac{1}{2}\Re(P \cdot \bar{\mathbf{U}}); \quad \mathbf{I_{in}} = \frac{1}{2}\Im(P \cdot \bar{\mathbf{U}}) \tag{10}$$

By then using the equation of the reactive intensity a relation can be obtained from the angle of reactive intensity with the real axis. Which would state the following relation:

$$tan(\theta_{I_{re}}) = tan(\frac{\alpha + \beta}{2}) \tag{11}$$

Here, α and β represent the average angles of the A and B waves and θ_{Ire} the angle of the reactive intensity. This implies that the average of the reactive intensity falls precisely in the middle of these waves. By applying the coordinate system rotation of $\theta_{I_{re}}$, the angles α' can be aligned with $-\beta'$. Here, α' and β' represent the angles between wave A and B in relation to the reactive intensity. A visualisation of this coordinate transformation is illustrated in Figure 2.

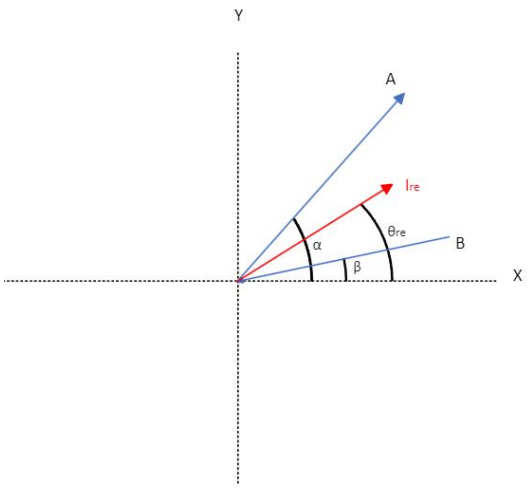

(a) A and B wave before rotating the coordinate system by $\theta_{I_{re}}$

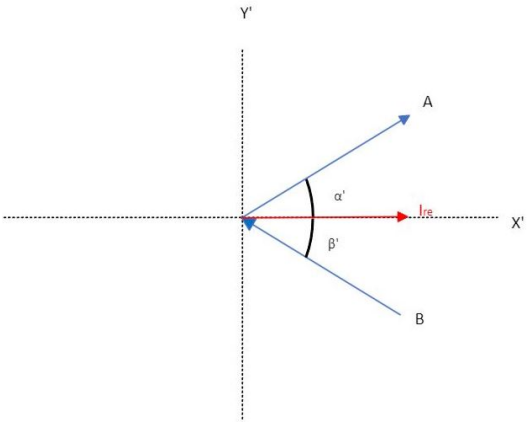

(b) A and B wave after rotating the coordinate system by $\theta_{I_{re}}$

Figure 2: Coordinate transformation of the A and B wave

By rotation of the coordinate system by θ_{re} the relation in velocity equations in the equations of 9 can be rewritten to an U'_x, U'_y, α' and become:

$$U'_x = \frac{1}{\rho c}((A-B)cos(\alpha')), \quad U'_y = \frac{1}{\rho c}((A+B)sin(\alpha')) \tag{12}$$

$$A = \frac{P}{2} + \frac{\rho c \cdot U'_x}{2cos(\alpha')}, \quad B = \frac{P}{2} - \frac{\rho c \cdot U'_x}{2cos(\alpha')} \tag{13}$$

$$\alpha' = sin^{-1}(\frac{\rho c \cdot U'_y}{P}), \quad with \quad U'_y = \frac{P}{\rho c} \cdot sin(\alpha') \tag{14}$$

So concluding, the first method discussed is called the Local Plane Wave (LPW) method, where the influence of the angle between the waves is not taken into account, the second method is called the Local Specular Plane Wave (LSPW) method where is taken into account that angle of the incoming wave is equal to the outgoing wave B. In the third and last discussed method is called the Plane Wave Decomposition(PWD) method where the angle between the in and outgoing wave can differ but still has some issues. All the methods which are researched can be seen visibly in Figure 3.

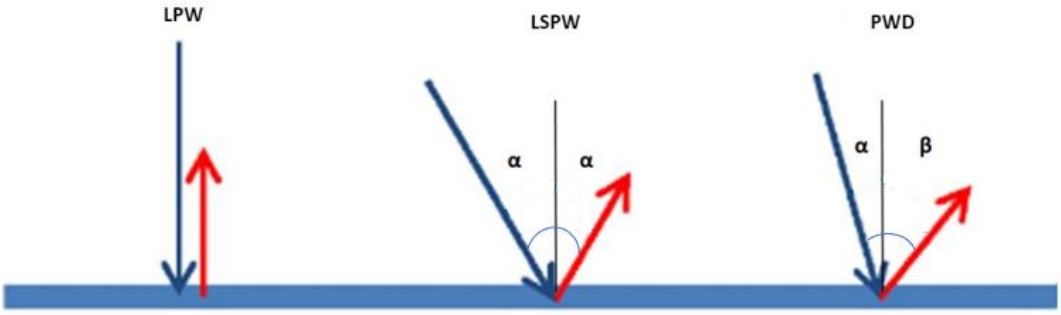

Figure 3: Illustration of the LPW, LSPW and PWD method

3.2 Analytical improvements

The method encounters problems when the value of $\sin(\alpha_r)$ exceeds 1 or $\sin(\alpha_r)$ falls below -1. In such instances, the angle between wave A and B is higher then 90° to the imaginary regime, leading to a function with a complex angle. To address this issue, a corrective action is introduced, involving a 90 degree angular adjustment under the condition that the argument of the inverse sin exceeds 1 or falls below -1. This adjustment is made based on the the suspicion that, in such instances, the waves behave differently and do not need to be altered to have the reactive intensity is already pointing in the real axis, prompting a strategic coordinate transformation to the imaginary axis. Therefore in the method, an 'if' function is invoked to address scenarios where the argument within the arcsine becomes exceeds one or falls below minus one, then the coordinate rotation must been set back to its original position.

By applying the 'if' function function into the code further simulations are made.

3.3 Deriving the covered area of the profile

In prior research [1] a simulation of the Louvre principle was conducted where a total area of dimensions 1000x500 millimeter is involved. The simulation focused on observing the dynamics of sound reflection and absorption within the Louvre principle, as it propagates throughout the given space. This approach was crucial for formulating the LPW method, as it provided insights into the acoustics by capturing the intensity of sound flowing in multiple directions. Method validation entails a comprehensive examination and needs to be rigorously tested across multiple parameters scattering, absorption, transmission and sound power if possible. To comprehensively validate across various parameters, different materials and structures can be incorporated within a defined space. For optimal configuration within a 3x3 meter area, optimal dimensions of 500x500 millimeter are recommended. Notably, these dimensions deviate from those used in the previous Louvre principle simulation, necessitating adjustments to the simulations.

3.4 The method used in 2D Simulations

In the process of method validation, a series of simulations has been systematically undertaken to ascertain its applicability. This section presents an in-depth analysis of three pivotal simulations, namely:

- Louvre door principle
- Test setup 2D
- Test setup 3D

Each setup undergoes testing across three distinct quantities, specifically focusing on the pressure field, velocity field and intensity field.

Louvre door principle

The Louvre principle is examined, establishing a connection with simulations conducted in prior research. Figure 4a illustrates the application of the PWD method in the louvre door simulation. However, in Figure 4b it is evident that in locations when the argument within the arcsine surpasses 1 or descends below -1 the calculation becomes impractical within the simulation software.

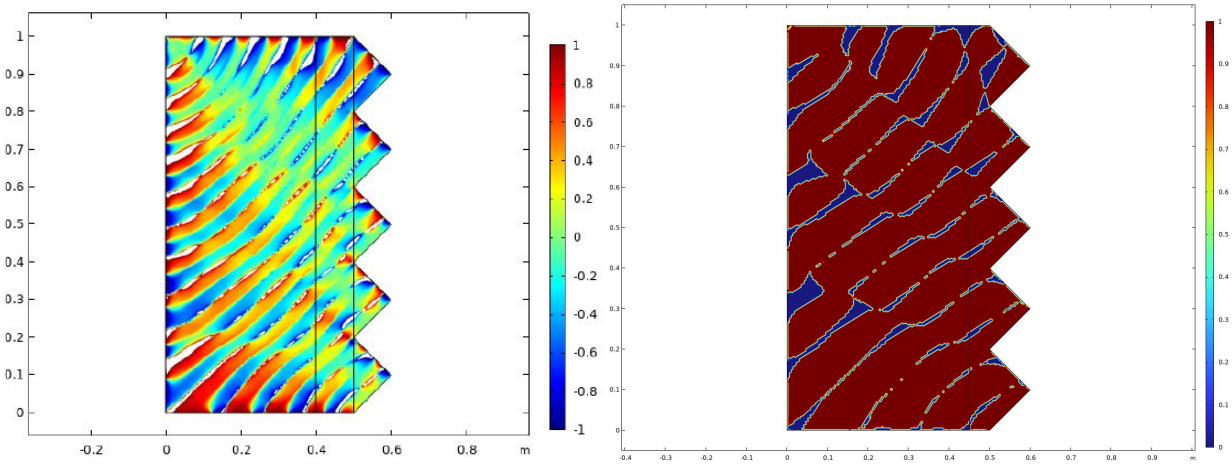

(a) 2D simulation louvre door arcsine ratio (b) 2D simulation ratio function higher then 1

Figure 4: 2D Simulation Louvre door

In Figure 5, the (if) function is implemented within the coordinate transformation. Upon closer examination of this simulation, it becomes evident that the arcsine is computed across the entire spatial domain.

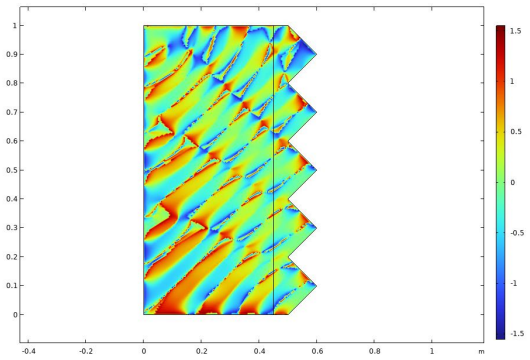

Figure 5: Simulation after extra coordination transformation

Having resolved this issue, a simulated 2D test setup is conducted in COMSOL. The spatial dimensions of this setup, spanning 500x500 square millimeters, as indicated by3.3, leading to the creation of a 2D test setup illustrated in Figure 6. The perimeter is enclosed by an aluminium BLOCAN profile, making to totally covered area 500x500 square millimeter. The details regarding the BLOCAN profile are discussed further in section 4.2.2 . In the left corner at the coordinates x= 0.02 y=0.02 a circular region with radius of 5 mm is positioned, designed to induce a controlled pressure. In this Figure the x axis is seen as the width and the y axis is seen as the length.

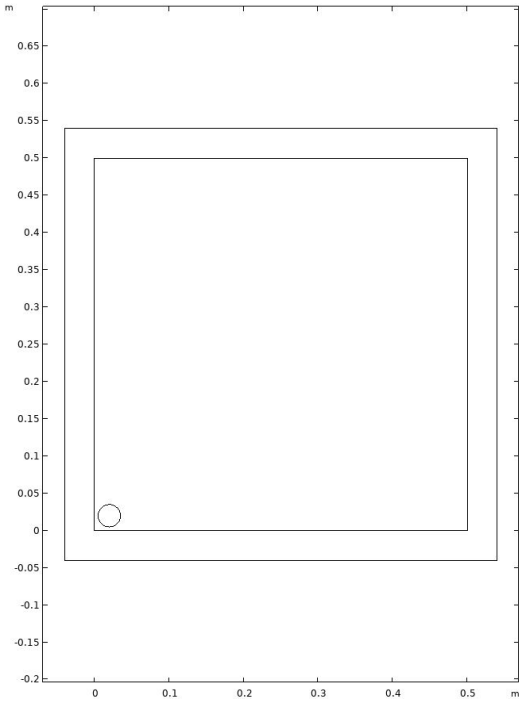

Figure 6: The test setup in 2D

The validation of the PWD method is done through simulations conducted in this 2D test setup. To ensure its applicability in real-word scenarios, a examination is conducted across key quantities, including:

- Pressure field
- Velocity in the x and y direction
- Intensity in the x and y direction

These quantities are systematically simulated in COMSOL, and their values are calculated as outlined in the method. Figure 7 illustrates two simulations of velocity field when a pressure is applied tho the circular region, showing the alignment between simulated and calculated values of the velocity field. The calculated values are made by applying the equations in equation 9. There must also be taken into account,for this situation, that the sin (α) is smaller then 1 for the whole field.

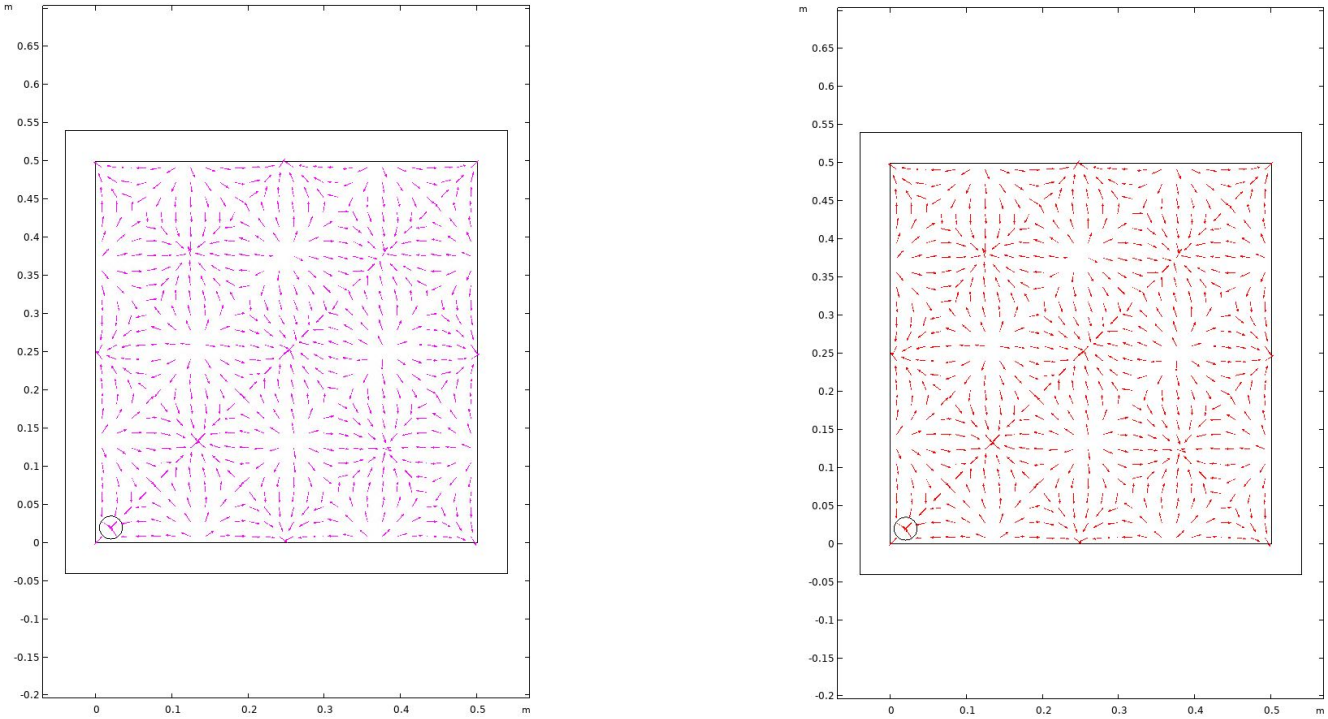

(a) 2D simulation velocity field simulated by COMSOL

(b) 2D simulation velocity field calculated through the PWD method

Figure 7: 2D simulation velocity field simulated by COMSOL and calculated through the PWD method

Figure 7a displays the simulated velocity field generated by COMSOL, while Figure 7b presents the calculated velocity field using the method. As the figures are identical, the validity of the method in accurately calculating a velocity field is proven. Similar outcomes are noted for both the pressure field and the intensity field. Therefore from a two dimensional perspective a broader validity across multiple key parameters is established.

3.5 Deriving the height of the space

To emulate a 2D scenario in a 3D setting, specific considerations must be made for the height in the spatial domain. The height of the spatial domain needs to be precisely defined to facilitate measurements, aligning with the nature of the 2D test setup. The formula that is important by selecting the height of the spatial domain is expressed as[5]:

$$2\lambda = \frac{c}{f} \tag{15}$$

Where the λ represent the length of a wave [m], c represents the speed of sound in [m/s] and f represents the frequency in [Hz]. Only two unknown parameters are presented and either of them has to be chosen for implementation of the 3D setup. For practical reasons the height is chosen to be 40 millimeters, as the height would represent half of the wave length in a two dimensional situation. The wave length (λ) is set to 80 millimeters.the results are as follows:

$$\lambda = \frac{c}{f} => f_{max} = \frac{343}{0.08} \simeq 4200[Hz] \tag{16}$$

Meaning maximum frequency the 3D setup facilitate is 4200 Hz in the frequency domain, with an the parameter of the height set to 40 millimeters. The spectrum of the frequency's to be looked at, is therefore set to 4000 Hz, in order to align with the nature of a 2D test setup.

3.6 3D Simulation

As detailed in section 3.5 a three-dimensional setup has been constructed with a height of 40 millimeters, what is designed to facilitate the functionality of a 2D nature. The simulated representation of the 3D test setup is presented in Figure 8 . Additional insights into the materials employed are provided in Chapter 4 and a comprehensive exploration of the simulation analysis methodology is expound in section 5.2 .

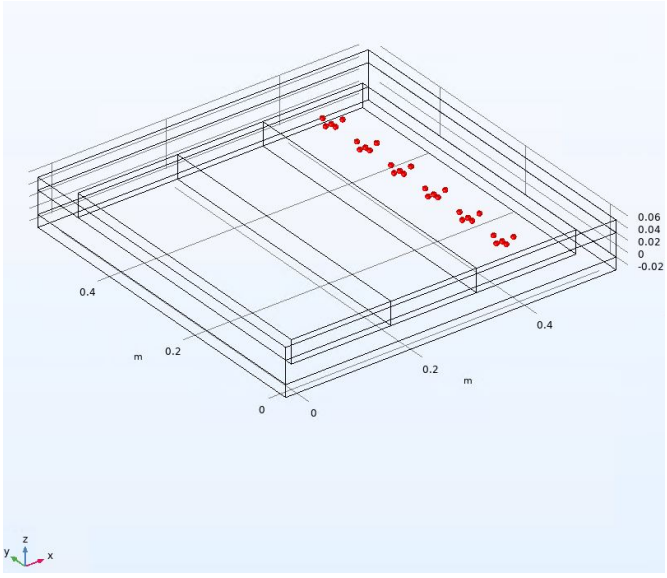

Figure 8: Simulation 3D test setup

4 The experimental test setup

While designing the experimental test setup, we examined how to realize the simulation made in COMSOL. It became known from the simulations that an area of 500x500 millimeter had to be covered and a chosen height of 40 millimeters to realize the 2D environment. These parameters are discussed in Chapter 2 and with these parameters a test setup is designed.

4.1 Designing the experimental test setup

In Figure 9 the designed experimental test setup can be seen. In Figure 9a the whole setup is shown including the top shelf, where in Figure 9b the top shelf is removed to see the inside of the setup. The microphones, speakers and measurement equipment cannot be seen in this figure as these parts are not made but are implemented in the experimental test setup.

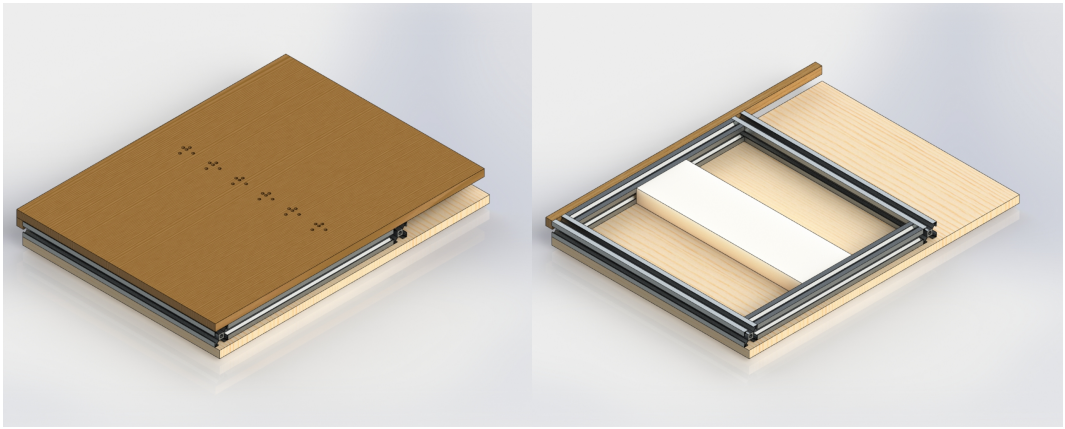

(a) Experimental test setup with top cover with material placed in the area

(b) Experimental test setup without top cover with material placed in the area

Figure 9: The experimental test setup

The following items are explained in this chapter

- The made experimental test setup
  - Functioning of the experimental test setup
  - BLOCAN profiel (aluminium)
- Choice of the microphones and sealing of the microphones
- Choice of source of the sound(speaker)
- Gathering of the data

Other tools apart from the experimental test setup that are used to create the simulated test setup are not explained here. These will be discussed in the further sections.

4.2 The test setup

The test setup exists of three parts, a wooden top plate, a wooden bottom plate and BLOCAN profiles. (In the figure it can be seen that a space with dimensions 500x500 millimeters is covered by an aluminium BLOCAN profile, which is enclosed on the top and bottom by a wooden plate with dimensions 800x600x21 millimeters.) This wooden plate at the bottom of the BLOCAN profile is connected to the BLOCAN profile by bolts.

4.2.1 Functioning of the experimental test setup

The microphones are placed into drilled holes on the topplate. These drilled holes can be seen in Figure 11a. The topplate is meant to move freely in it's x direction to the positions as can be seen in Figure 10. In the position of Figure 10a the microphones are placed within the area at x1=400(as it maximum position) and can move to position x2=167(as it minimum position) as can be seen in Figure 10b. Which means the measurements can be done freely between x1=400 and x2=167, when measuring displacement with a ruler along the x axis. To ensure that the plate will only move in its x-direction a small wooden beam is connected to the top wooden plate on its edge in the width by screws.

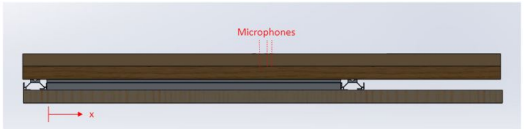

(a) Microphones at its maximum distance placed from the speaker

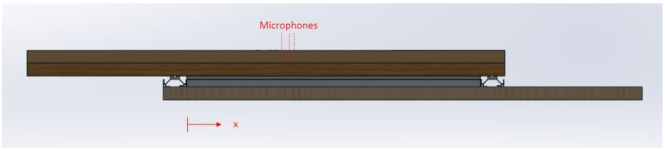

(b) Microphones at its minimum distance placed from the speaker

Figure 10: Maximum and minimum position of the microphones

As said, the measurements are done via microphones which are mounted into the holes which are drilled along a y-axis, as illustrated in Figure 11a. A microphone is mounted in each hole. Six sets of five holes can be recognized in the Figure 11a and one set of five microphones is illustrated in Figure 11b. The measurements of these microphones are analysed in section 5.1. From these analyses, the pressure is measured and particle velocity in the x direction are approximated.
When microphones are used from multiple sets, of each five microphones, the particle velocity can be approximated(more is explained in section 5.1) for various position in the area of the six sets. This will help to yield a more clear view of the pressure and particle velocity in the area between x2=167 and x1=400.

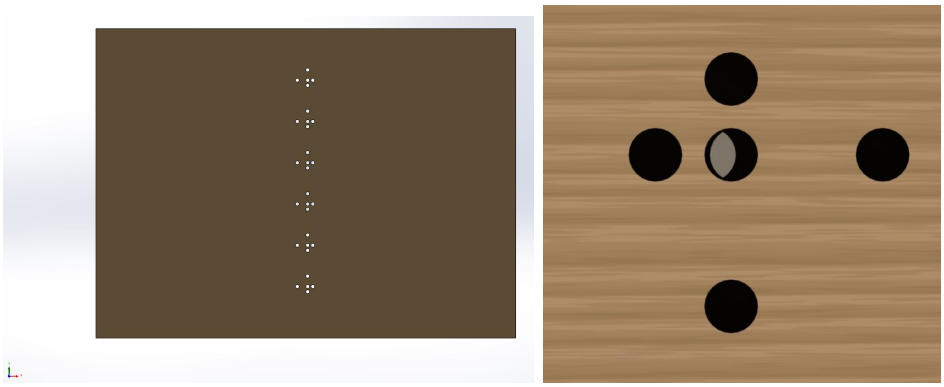

(a) Topview topplate (b) One microphone set

Figure 11: Microphone set

4.2.2 BLOCAN profile

From the simulated test setup it is derived that a space of 500x500x40 millimeter air is needed. A BLOCAN profile is made of aluminium and therefore the most practical solution for the experimental setup considering the characteristics(reflection coefficient, density, etc) of the material and the availability of these profiles in the laboratory . Multiple sizes of BLOCAN profile are available in the laboratory, so the space size can easily be adjusted if needed. In Figure 12 the BLOCAN profile is shown that is used in the experimental test setup.

Figure 12: The BLOCAN profile

4.2.3 Sealing of the microphones

We decided to install the microphones on top of the experimental test setup. Because of this construction it will be more easy, due to the gravity, to seal the microphones and mounting of the microphones is more safe. The holes, where the microphones a put through, where drilled at a tight fit(a diameter of 7.2 millimeter). Because of this tight fit the microphone had already a good sealing and had a low chance of dropping due to gravity. However, because of the relative high price of the microphones, a sealing was

designed to lock each microphone at it's place, preventing the microphone from dropping to the lower surface. The designed lock can be seen in Figure 13 .

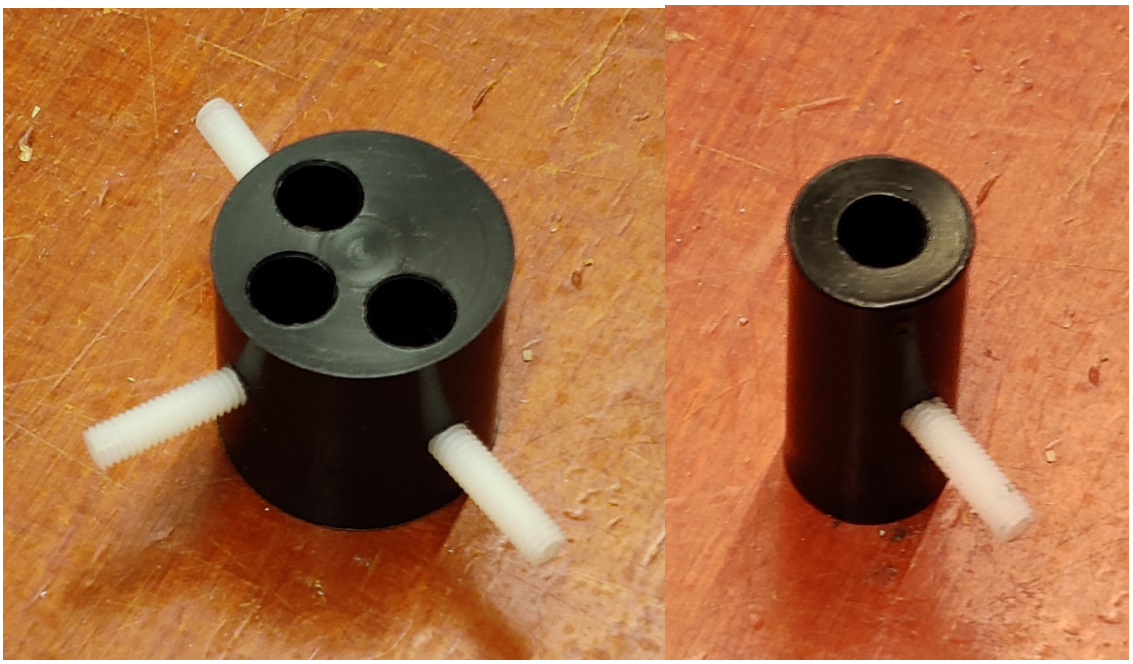

(a) Lock for three microphones (b) Lock for one microphone

Figure 13: Locks used for the microphones

4.2.4 Choice of speaker

A source of the sound is needed to reconstruct the source of sound from the simulation setup. To realise this source of sound a speaker is installed into the experimental setup. By making the choice for the speaker the following criteria has to be kept in mind:

- The sound source may have little to no influence on it's surrounding material.
- The length of the cone of the speaker must have a maximum of 175 millimeter, so objects still can be placed at the center of the space in the experimental test setup.
- For safety reasons the speaker must have a maximum sound production of 80 dB at the position of the operator.

Multiple speakers posses these criteria but due to specifications about size and the frequency response of the speaker, the 'Visaton BF 32'[6] is chosen and installed in the experimental test setup, as can be seen in Figure 14a. An amplifier is needed in order for this speaker to produce sound. The amplifier(used from the laboratory) can be seen in Figure 14b. Specifications of the speaker and the amplifier can be found in the appendix B.

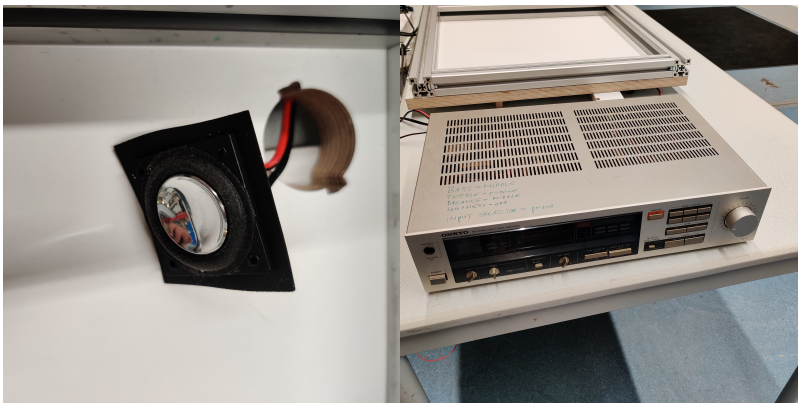

(a) Speaker in corner (b) Amplifier

Figure 14: Speaker setup

4.2.5 Acquiring data from the microphones to the computer

The measurements in the experimental test setup are done via the 'GRAS40PH' microphones[7]. The specifications of these microphones are given in appendix C. With the knowledge of these chosen microphones an experimental test setup is designed.

The data is measured through 'Grass 40PH microphones' which are installed on top of the top plate as can be seen in Figure 15 .

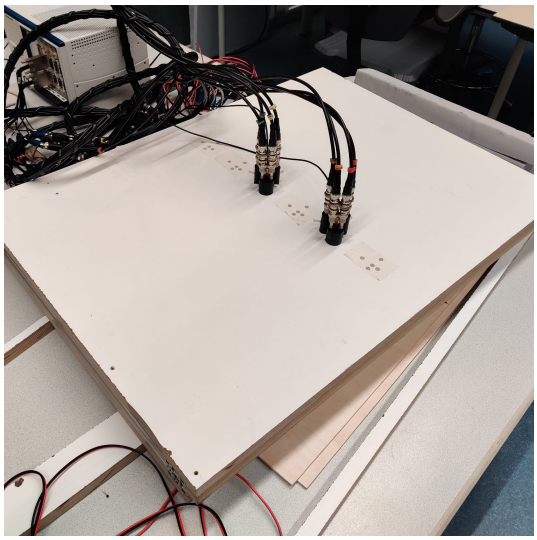

Figure 15: Two microphone sets, of each five microphones, on top of the top plate

Because of the rigid configurations of the cable only two microphone sets can be installed on the top plate. This cable connects the microphones to a PXIe system. So the measurements of the microphones are done with two sets of microphones at the same time. The other holes on the top plate are sealed with masking tape from both ends of the hole to avoid leakage .
The microphones are connected to a PXIe system [8] which transfers the data ,via a LABVIEW driven software, in a TDMS file. The data in the TDMS file must be converted into a h5 file. This converted h5

file can be imported in MATLAB and give the required pressure data, which is used in the calculation. The further calculation, to acquire the results about the experimental test setup, done via MATLAB, is then used in the equations and defines a pressure distribution in a frequency domain as can be seen in Figure 16 .

Figure 16: Setup to acquire the data

5 Analyses

The data gathered from the made simulations in COMSOL and the data gathered by the experimental test setup is analysed in order to gain the quantities by mean of implementing of the LPW method. This analyses regarding the simulated setup is done in 5.2 and the analyses for the experimental test setup is done in section 5.1.

5.1 Analysing the data

When looking at the experimental test setup, from the top, the holes on the top plate ,are placed in six sets of each five holes. In Figure 17, it is shown how the sets are distributed along the top plate.

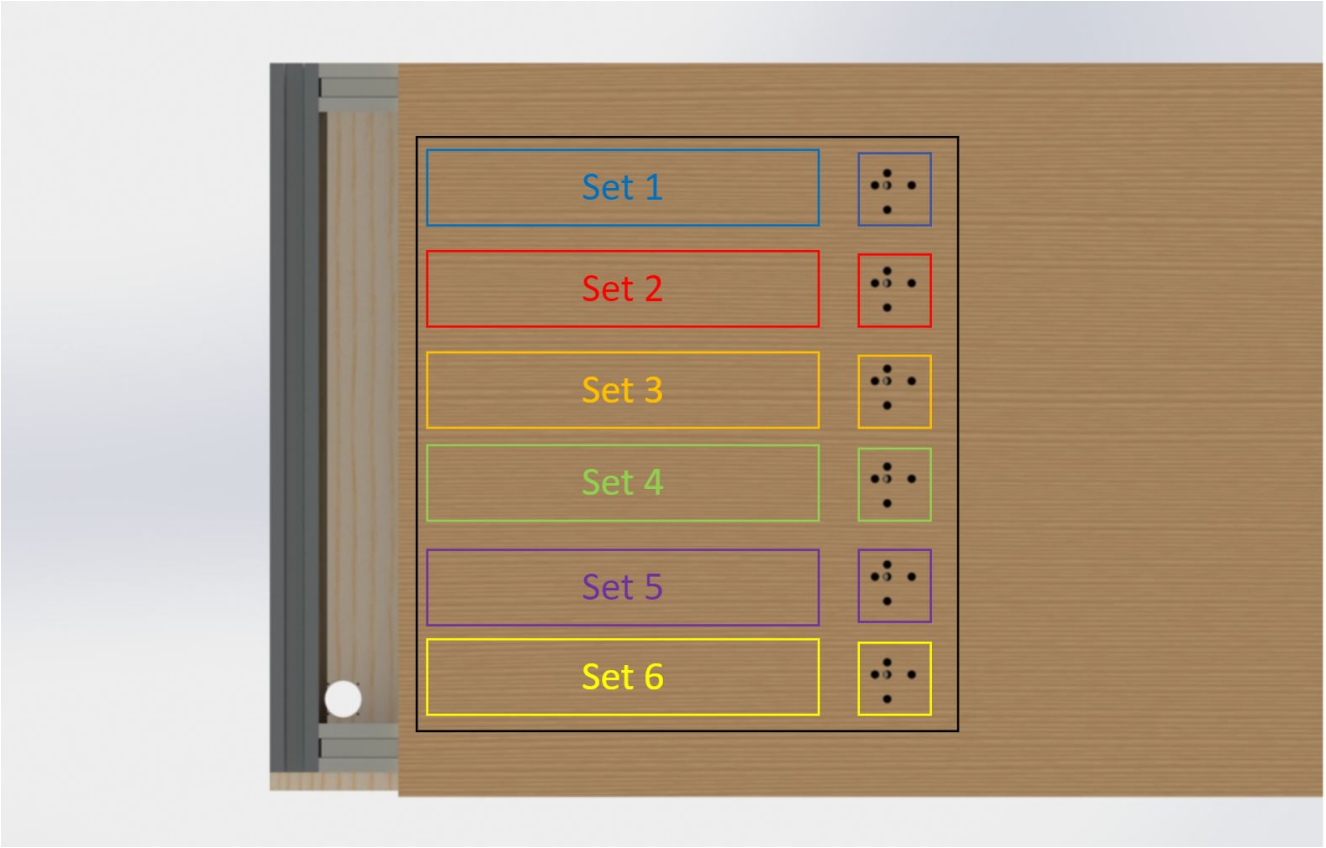

Figure 17: The microphones grouped in sets of five, distributed six times

A detailed view of one set is illustrated in Figure 11b. The microphones are placed in these holes and measure a pressure difference. For simplicity the microphones can also be seen as five different measured pressures. For practical reasons these are described as P_{1x}, P_{1y}, P_2, P_{3x}, P_{3y}. The locations of the measured pressures are illustrated in Figure 18 .

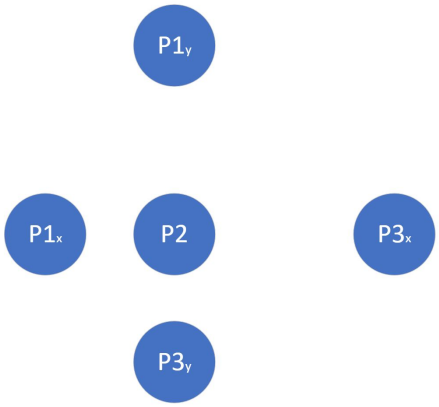

Figure 18: Measure pressure from microphones

As mentioned in the first chapter the following quantities need to be calculated or measured:

- Pressure (P)
- Particle velocity in x and y direction (U_x and U_y)
- Intensity in x and y direction (I_x and I_y)

The absorption coefficient must be calculated from the last quantity (intensity).
The microphones measure the pressure, meaning the first quantity is measured. The formula for the particle velocity is:

$$U_x = \frac{i}{\rho\omega} \cdot \frac{\partial P}{\partial x} \tag{17}$$

The data measured by the microphones are translated to a frequency domain so the ω can be calculated with the formula $\omega = 2\pi f$. The test are measured in an environment of air, the density of air(ρ) is known. So only the $\frac{\partial P}{\partial x}$ needs to be calculated.
The formulas for the incident intensity and the active intensity with the use of the LPW method are:

$$I_{in} = \frac{A\bar{A}}{2\rho c} \quad , \quad \mathbf{I_{ac}} = \frac{1}{2}\Re(P \cdot \overline{\mathbf{U} \cdot \mathbf{n}}) \tag{18}$$

From the theory in section 3 the formula for wave A is:

$$A = \frac{1}{2}(P + \rho c \mathbf{U} \cdot \mathbf{n}) \tag{19}$$

So the formula for the incident intensity is:

$$I_{in} = \frac{1}{2\rho c}(P + \rho c \mathbf{U} \cdot \mathbf{n})(\overline{P} + \rho c \overline{\mathbf{U} \cdot n}) \tag{20}$$

This shows that only the pressure and particle velocity are needed to calculate the incident intensity. So far the particle velocity is unknown. This can be calculated as will be shown in the next subsection.

5.1.1 Calculation of the incident intensity

In both the x and y direction three microphones are aligned to each other. The $\frac{\partial P}{\partial x}$ can be measured between two points by using two microphones. By using three aligned microphones, the particle velocity in the centre microphone can be measured more accurate. So there are two methods to approximate the particle velocity which will be further explained in this section.

5.1.2 Calculating incident intensity using two microphones

By choosing two microphones the particle velocity is approximated in the exact middle of these two microphones. An absorbing material is placed in the area along the whole y axis between x=200 and x=363, which means the sound(which is produced at x=0) will be propagating in the x direction. So therefore, we chose to align the microphones on the x axis. The chosen microphones are shown in Figure 19, which are P_{1x} and P_{2x}, where the distance between these microphones is equal to D1.

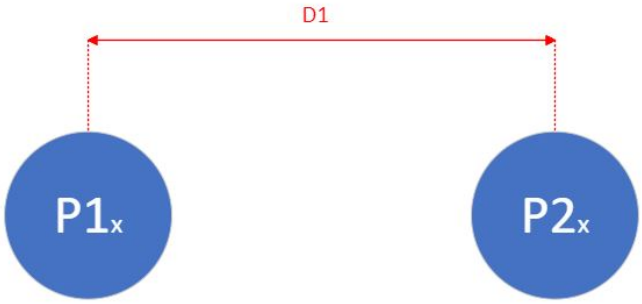

Figure 19: Two microphones

Now $\frac{\partial P}{\partial x}$ can be written as $\frac{P_{2x}-P_{1x}}{D1}$, so the formula for the U_x is(when using two microphones):

$$U_x = \frac{i}{\rho\omega}\frac{P_{2x}-P_{1x}}{D1} \tag{21}$$

When adding this into the equation for the incident intensity, the equation becomes:

$$I_{in} = \frac{1}{2\rho c}\big(\frac{1}{2}(P + \rho c\frac{i}{\rho\omega}\frac{P_{2x}-P_{1x}}{D1})\big)\big(\frac{1}{2}(\overline{P}_{2x} + \rho c\overline{\frac{i}{\rho\omega}\frac{P_{2x}-P_{1x}}{D1}})\big) \tag{22}$$

Which can be written as:

$$I_{in} = \frac{1}{8\rho c}(P_{2x} + \frac{i}{k}\frac{P_{2x}-P_{1x}}{D1})(\overline{P}_{2x} + \frac{-i}{k}\overline{\frac{P_{2x}-P_{1x}}{D1}}) \tag{23}$$

Where $k = \frac{\omega}{c}$ denotes the wave number. To do the calculation, the terms in the brackets can be written

in four terms:

$$I_{in} = \frac{1}{2\rho c}\Big(\underbrace{P_{2x}\overline{P}_{2x}}_{\text{term1}} + \underbrace{P_{2x}\frac{-i}{k}\frac{\overline{P_{2x}-P_{1x}}}{D1}}_{\text{term2}} + \underbrace{\frac{i}{k}\frac{P_{2x}-P_{1x}}{D1}\overline{P}_{2x}}_{\text{term3}} + \underbrace{\frac{i}{k}\frac{P_{2x}-P_{1x}}{D1}\frac{-i}{k}\frac{\overline{P_{2x}-P_{1x}}}{D1}}_{\text{term4}}\Big) \tag{24}$$

For better understanding the equation is divided into four terms. Term two and term three can be described as:

$$term2 = \frac{-i}{k}\frac{P_{2x}\overline{P}_{2x} - P_{2x}\overline{P}_{1x}}{D1} \quad , \quad term3 = \frac{i}{k}\frac{P_{2x}\overline{P}_{2x} - P_{1x}\overline{P}_{2x}}{D1} \tag{25}$$

And term four can be written as:

$$term4 = \frac{1}{k^2}\frac{P_{2x}\overline{P}_{2x} - P_{1x}\overline{P}_{2x} - P_{2x}\overline{P}_{1x} + P_{1x}\overline{P}_{1x}}{D1^2} \tag{26}$$

So the incident intensity is:

$$I_{in} = \frac{1}{2\rho c}\Big(P_{2x}\overline{P}_{2x} + \frac{-i}{k}\frac{P_{2x}\overline{P}_{2x} - P_{2x}\overline{P}_{1x}}{D1} + \frac{i}{k}\frac{P_{2x}\overline{P}_{2x} - P_{1x}\overline{P}_{2x}}{D1} + \frac{1}{k^2}\frac{P_{2x}\overline{P}_{2x} - P_{1x}\overline{P}_{2x} - P_{2x}\overline{P}_{1x} + P_{1x}\overline{P}_{1x}}{D1^2}\Big) \tag{27}$$

When writing the incident intensity in the terms of $P_{...x}\overline{P_{...x}}$ the equation for MATLAB becomes:

$$I_{in} = \frac{1}{2\rho c}\Big(P_{2x}\overline{P}_{2x}(1 + \frac{1}{k^2D1^2}) + P_{2x}\overline{P}_{1x}(\frac{i}{kD1} - \frac{1}{k^2D1}) + P_{1x}\overline{P}_{2x}(\frac{-i}{kD1} - \frac{1}{k^2D1^2}) + \frac{P_{1x}\overline{P}_{1x}}{k^2D1^2}\Big) \tag{28}$$

5.1.3 Method using three microphones

By analysing the particle velocity with three microphones, the microphones are aligned along on the x axis, which is done for practical reasons explained in the first paragraph of section 5.1.2. The chosen microphones are shown in Figure 20 which are P_{1x}, P_{2x} and P_{3x}. The distance between P_{1x} and P_{2x} is equal to D1 and the distance between P_{2x} and P_{3x} is equal to D2. To approximate the pressure in P_{2x}.

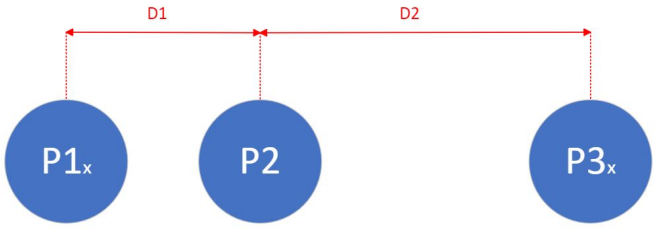

Figure 20: Three microphones

The $\frac{\partial P}{\partial x}$ can be derived by using matrix manipulations. The equation becomes:

$$\begin{pmatrix} P_{2x} \\ \frac{\partial P_{2x}}{\partial x} \\ \frac{\partial^2 P_{2x}}{\partial x^2} \end{pmatrix} = \begin{pmatrix} 1 & 0 & 0 \\ 1 & D1 & D1^2 \\ 1 & D2 & D2^2 \end{pmatrix}^{-1} \times \begin{pmatrix} P_{2x} \\ P_{1x} \\ P_{3x} \end{pmatrix} \tag{29}$$

By means of MATLAB, $\frac{\partial P_{2x}}{\partial x}$ is determined as:

$$\frac{\partial P_{2x}}{\partial x} = \frac{(D2^2 - D1^2)P_{2x} + D1^2 P_{1x} - D2^2 P_{3x}}{D1D2(D1 - D2)} \tag{30}$$

which can be filled into the equation for the particle velocity:

$$U_x = \frac{i}{\rho\omega} \frac{(D2^2 - D1^2)P_{2x} + D1^2 P_{1x} - D2^2 P_{3x}}{D1D2(D1 - D2)} \tag{31}$$

When this is filled in equation 21 the formula for the incident intensity becomes:

$$I_{in} = \frac{1}{2\rho c}\big(P_{2x} + \rho c \frac{i}{\rho\omega} \frac{(D2^2 - D1^2)P_{2x} + D1^2 P_{1x} - D2^2 P_{3x}}{D1D2(D1 - D2)}\big)\big(\overline{P_{2x}} + \rho c \overline{\frac{i}{\rho\omega} \frac{(D2^2 - D1^2)P_{2x} + D1^2 P_{1x} - D2^2 P_{3x}}{D1D2(D1 - D2)}}\big) \tag{32}$$

once the equation has been expanded further, the formula can be divided into four terms:

$$\begin{aligned} I_{in} = \frac{1}{2\rho c}\Big(& \underbrace{P_{2x}\overline{P}_{2x}}_{\text{term1}} + \underbrace{P_{2x}\frac{-i}{k}\overline{\frac{(D2^2 - D1^2)P_{2x} + D1^2 P_{1x} - D2^2 P_{3x}}{D1D2(D1 - D2)}}}_{\text{term2}} \\ & + \underbrace{\frac{i}{k}\frac{(D2^2 - D1^2)P_{2x} + D1^2 P_{1x} - D2^2 P_{3x}}{D1D2(D1 - D2)}\overline{P}_{2x}}_{\text{term3}} \\ & + \frac{1}{k^2}\underbrace{\frac{(D2^2 - D1^2)P_{2x} + D1^2 P_{1x} - D2^2 P_{3x}}{D1D2(D1 - D2)}\overline{\frac{(D2^2 - D1^2)P_{2x} + D1^2 P_{1x} - D2^2 P_{3x}}{D1D2(D1 - D2)}}}_{\text{term4}}\Big) \end{aligned} \tag{33}$$

Upon expanding the terms:

$$
\begin{aligned}
term1 =& P_{2x}\overline{P_{2x}} \\
term2 =& \frac{-i}{k}\frac{(D2^2-D1^2)P_{2x}\overline{P_{2x}}+D1^2P_{2x}\overline{P_{1x}}-D2^2P_{2x}\overline{P_{3x}}}{D1D2(D1-D2)} \\
term3 =& \frac{i}{k}\frac{(D2^2-D1^2)P_{2x}\overline{P}_{2x}+D1^2P_{1x}\overline{P}_{2x}-D2^2P_{3x}\overline{P}_{2x}}{D1D2(D1-D2)} \\
term4 =& \frac{1}{k^2}\Big(\frac{(D2^2-D1^2)\big((D2^2-D1^2)P_{2x}\overline{P}_{2x}-D1^2P_{2x}\overline{P}_{3x}+D2^2P_{2x}\overline{P}_{1x}\big)}{(D1D2(D1-D2))^2} \\
&+\frac{D1^2\big((D2^2-D1^2)P_{1x}\overline{P}_{2x}+D1^2P_{1x}\overline{P}_{3x}-D2^2P_{1x}\overline{P}_{1x}\big)}{(D1D2(D1-D2))^2} \\
&+\frac{D2^2\big((D2^2-D1^2)P_{3x}\overline{P}_{2x}-D1^2P_{3x}\overline{P}_{3x}+D2^2P_{3x}\overline{P}_{1x}\big)}{(D1D2(D1-D2))^2}\Big)
\end{aligned}
\tag{34}
$$

So the incident intensity is:

$$
\begin{aligned}
I_{in} = \frac{1}{2\rho c}\Bigg(& P_{2x}\overline{P_{2x}} \\
&+\frac{-i}{k}\frac{(D2^2-D1^2)P_{2x}\overline{P_{2x}}+D1^2P_{2x}\overline{P_{1x}}-D2^2P_{2x}\overline{P_{3x}}}{D1D2(D1-D2)} \\
&+\frac{i}{k}\frac{(D2^2-D1^2)P_{2x}\overline{P}_{2x}+D1^2P_{1x}\overline{P}_{2x}-D2^2P_{3x}\overline{P}_{2x}}{D1D2(D1-D2)} \\
&+\frac{1}{k^2}\Big(\frac{(D2^2-D1^2)\big((D2^2-D1^2)P_{2x}\overline{P}_{2x}-D1^2P_{2x}\overline{P}_{3x}+D2^2P_{2x}\overline{P}_{1x}\big)}{\big(D1D2(D1-D2)\big)^2} \\
&+\frac{D1^2\big((D2^2-D1^2)P_{1x}\overline{P}_{2x}+D1^2P_{1x}\overline{P}_{3x}-D2^2P_{1x}\overline{P}_{1x}\big)}{\big(D1D2(D1-D2)\big)^2} \\
&+\frac{D2^2\big((D2^2-D1^2)P_{3x}\overline{P}_{2x}-D1^2P_{3x}\overline{P}_{3x}+D2^2P_{3x}\overline{P}_{1x}\big)}{\big(D1D2(D1-D2)\big)^2}\Big)\Bigg)
\end{aligned}
\tag{35}
$$

When writing the equation of the incident intensity in terms of $P_{...x}\overline{P_{...x}}$ in MATLAB, then equation 36 is realised. In this equation the terms of d_3 and d_4 are respectively: $d_3 = D2^2-D1^2$ and $d_4 = D1D2(D1-D2)$.

$$
\begin{aligned}
I_{in} = \frac{1}{2\rho c}\Big(& P_{2x}\overline{P_{2x}}\big(1+\frac{d_3^2}{d_4^2}\big)+P_{2x}\overline{P_{1x}}\big(\frac{-iD2^2}{d_4k}+\frac{d_3D2^2}{k^2d_4^2}\big)+P_{2x}\overline{P_{3x}}\big(\frac{iD2^2}{d_4}-\frac{d_3D1^2}{k^2d_4^2}\big) \\
&+P_{1x}\overline{P}_{2x}\big(\frac{iD1^2}{d_4}+\frac{D1^2d_3}{k^2d_4^2}\big)+P_{3x}\overline{P}_{2x}\big(\frac{-iD2^2}{kd_4}+\frac{D2^2d_3}{k^2d_4^2}\big)+P_{1x}\overline{P}_{3x}\big(\frac{D1^4}{k^2d_4^2}\big) \\
&P_{3x}\overline{P}_{1x}\big(\frac{D2^4}{k^2d_4^2}\big)+P_{1x}\overline{P}_{1x}\big(\frac{-D2^2D1^2}{k^2d_4^2}\big)+P_{3x}\overline{P}_{3x}\big(\frac{-D1^2D2^2}{k^2d_4^2}\big)\Big)
\end{aligned}
\tag{36}
$$

5.1.4 Calculation of the absorption coefficient

The absorption coefficient can be calculated with the active intensity and the incident intensity. In Figure 21 an illustration is given about the direction of the waves:

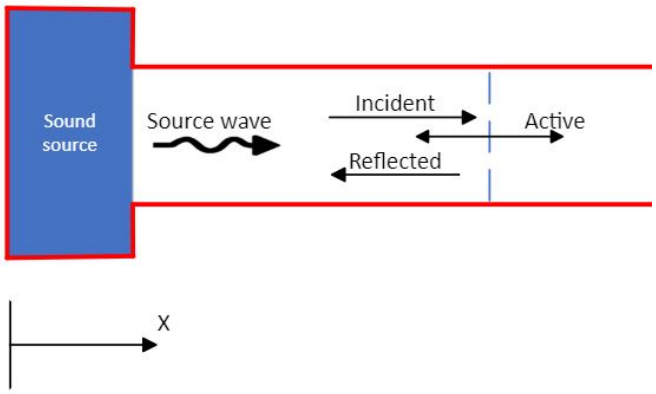

Figure 21: Illustration of a body with a partly enclosed sound source generating a sound wave in the positive x direction and an output on the other side. The incident wave is directed in the positive x direction, the reflective wave is directed in the negative x direction. The direction of the active wave can either be in the positive or in the negative x direction.

Figure 21 indicates that the active wave is either directed in the positive or negative x direction. By calculating the absorption coefficient(α), an 'if' function must be applied resulting in the following equations:

$$I_{ac} > 0 \quad => \quad \alpha = \frac{I_{ac}}{I_{in}}, \tag{37}$$

$$I_{ac} < 0 \quad => \quad \alpha = \frac{-I_{ac}}{I_{refl}} \tag{38}$$

This results in either a negative or positive absorption coefficient. The I_{refl} can be calculated similarly as the calculation of the I_{in} only the I_{refl} is based on the B wave instead of the A wave. This results in the following equations:

$$I_{in} = \frac{A\overline{A}}{\rho c} \quad , \quad I_{refl} = \frac{B\overline{B}}{\rho c} \tag{39}$$

So far I_{in} and I_{refl} are calculated, but I_{ac} is still unknown and must be calculated. The formula for the active intensity is:

$$I_{ac} = \frac{1}{2}\Re(P \cdot \overline{\mathbf{U}}) \tag{40}$$

Which can be written for this situation as:

$$I_{ac} = \frac{1}{2}\Re(P_{2x} \cdot \overline{U_x}) \tag{41}$$

The term within the brackets is identical to the term 3 used in equation 33 where $P_{2x} \cdot \overline{U_x}$ is already described. So the formula for the active intensity then becomes:

$$I_{ac} = \frac{1}{2}\Re\Big(\frac{i}{k}\frac{(D2^2 - D1^2)P_{2x}\bar{P}_{2x} + D1^2 P_{1x}\bar{P}_{2x} - D2^2 P_{3x}\bar{P}_{2x}}{D1D2(D1 - D2)}\Big) \tag{42}$$

With all quantities now known, the absorption coefficient can be determined. The results of the calculations are shown in Chapter 6 .

5.2 Analysing the simulated test setup

The data needed from the simulated test setup can be obtained of the COMSOL simulation. This is done by setting multiple points into the perimeter on the identical locations where the measurements are executed in the experiments. This shown in Figure 22.

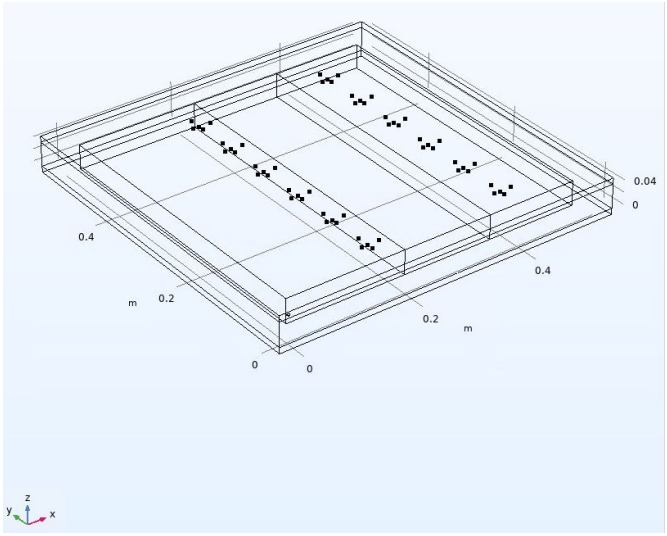

Figure 22: Simulated measured points in the simulated test setup

COMSOL already calculates the following quantities in a point:

- The pressure
- The particle velocity in the x and y direction
- The sound intensity in the x and y direction

The calculations of the A and the B wave, I_{in}, I_{refl}, I_{ac} and the absorption coefficient (α) must be done manually in COMSOL. This can be done by specifying quantities as variables in COMSOL.

6 Results

A total of eight experiments have been done to check whether the PWD method would hold in the experimental test setup. This is done by placing melamine foam into the cavity. Three measurements are done, in which the foam has different thicknesses, and one measurement is done with no foam in the (empty)space. The different thicknesses of the foam are 50 millimeter, 100 millimeter and 150 millimeter. The foam is placed at a distance of x=200. The measurements are repeated at the maximum distance from the source and at the minimal distance from the source. With these measurements the three quantities are calculated and could proof if the PWD method would be a valid method. These quantities are:

- Sound pressure level(L_p)
- Velocity level(L_v)
- Absorption coefficient(Intensity)

These quantities are discussed in this chapter.

6.1 Results L_P(Pressure) & L_v(Velocity)

In Figure 23, the results regarding the sound pressure level(L_p) and the velocity level(L_p) of microphone set 4 are shown. The other results regarding the sound pressure level(L_p) and the velocity level(L_p) are shown in the Figure 39 and Figure 40, in appendix. In these figures, a graph of the values of the L_p and the L_v from the simulations and the measurements are shown for all six microphone sets. The measurements are executed near the speaker where no material is added to the space. The L_p is calculated according to:

$$L_p = 10log(\frac{p_{rms}^2}{p_{ref}^2}) \quad [dB] \quad with \quad p_{ref} = 2 \cdot 10^{-5}[Pa] \tag{43}$$

The L_v is calculated by mean of following formula:

$$L_v = 10log(\frac{v_{rms}^2}{v_{ref}^2}) \quad [dB] \quad with \quad v_{ref} = 5 \cdot 10^{-8}[m/s][9] \tag{44}$$

In the graphs, the results of the L_P and the L_v of the experiments and the simulation are displayed and show no relation. Even the results of the velocity level shows a level difference of more then 30 dB. The big difference between the simulations and the experiments may be caused by difficulties in the representation of the speaker in the software. In the simulation a pressure or velocity point source is added as replacement of the speaker. The absorption coefficient of the experiments and the simulations should show resemblance. The difference in the L_p and the L_v does not affect the absorption coefficient as this quantity is not fully dependant on either the pressure or the particle velocity. The results of the absorption coefficient can be found in section 6.2.

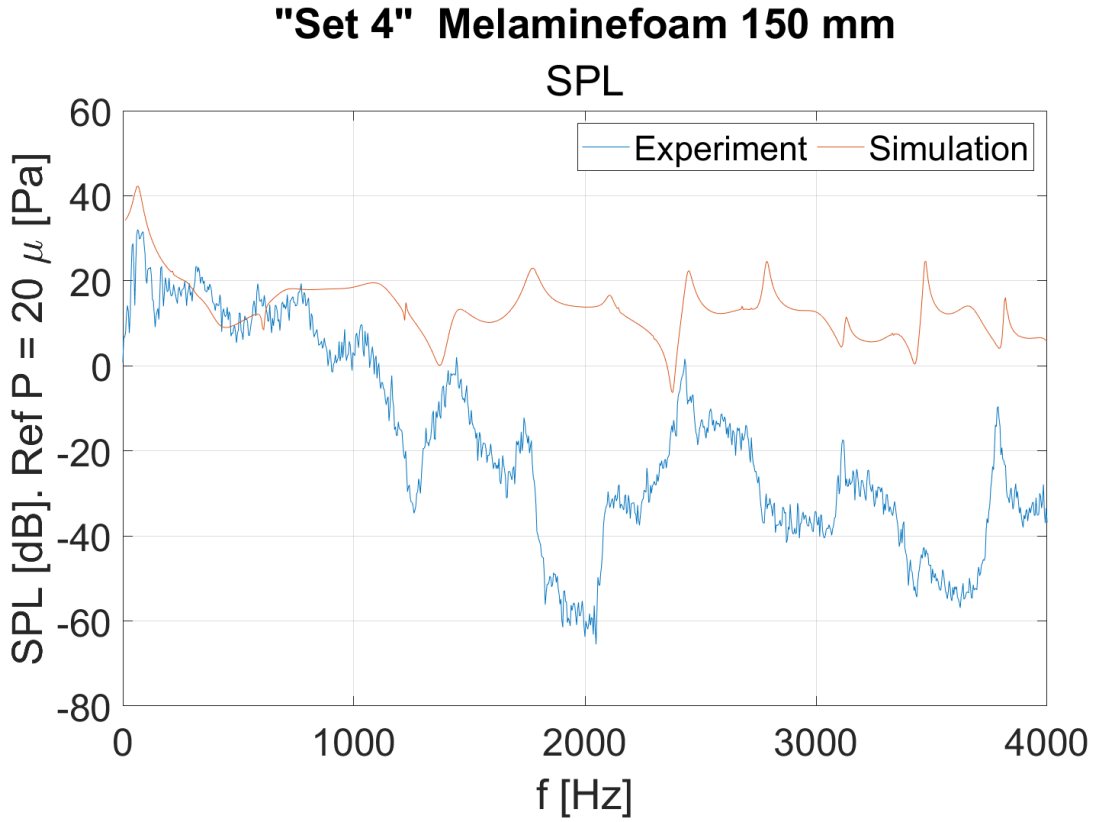

(a) Results of the L_p of microphone set 4 placed at a minimal distance to the source where melamine foam, width 150 millimeter, is added into the cavity of the experimental test setup and the simulated test setup.

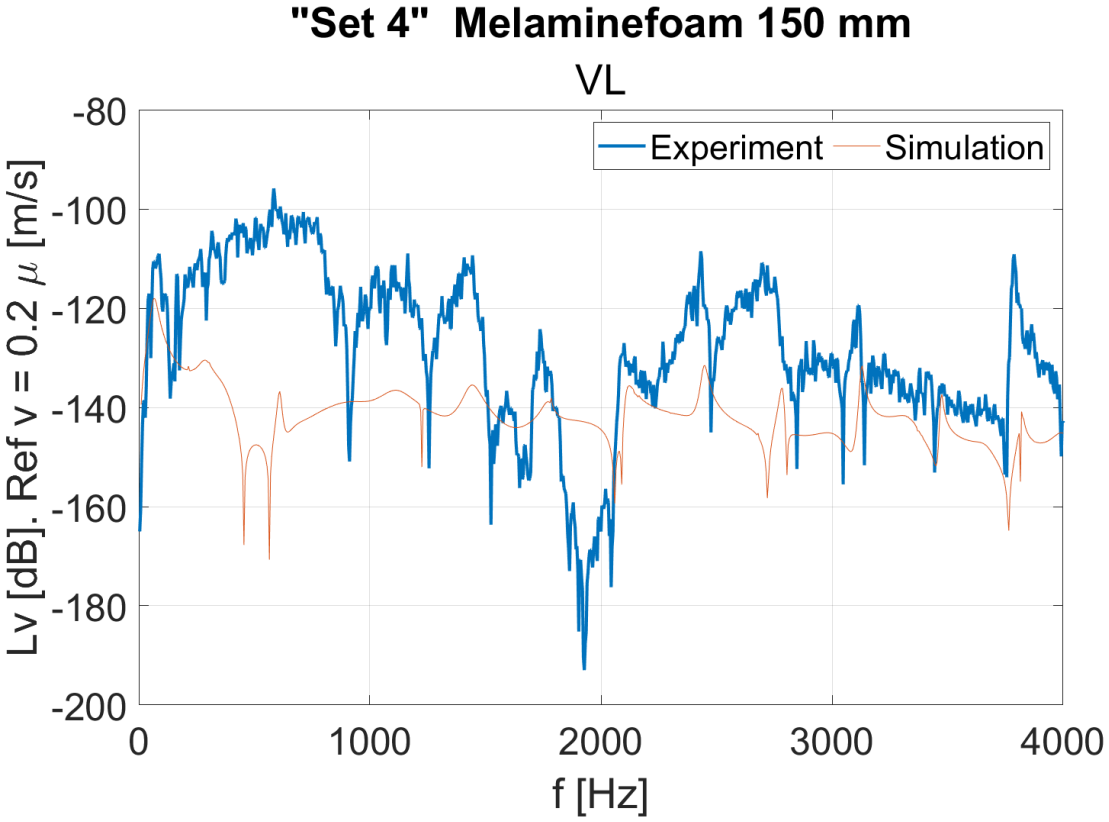

(b) Results of the L_v of microphone set 4 placed at a minimal distance to the source where melamine foam, width 150 millimeter, is added into the cavity of the experimental test setup and the simulated test setup.

Figure 23: Example of the L_p and the L_v measured vs simulation along the six microphone sets at a minimal distance to the sound source with 150mm melamine foam placed in the test setup.

6.2 Results absorption coefficient

In chapter 5, it is shown how the absorption coefficient can be calculated. The results of melamine foam, with a width of 150 millimeter, added into the space are shown in Figure 24 and Figure 25. The microphones are placed near the speaker for the results in Figure 24 and the microphones are placed at the furthest point away from the speaker for the results in Figure 25. The results shown are realised with the method using three microphones. The differences between the two methods are shown in subsection 6.2.1.

In Figure 24 it can be seen that the absorption coefficient is quite high(close to one) for most frequency's. It is expected that little to no sound would be measured at the microphones that are placed behind the melamine foam. So it is expected that the absorption coefficient at the furthest point of the source of sound would be close to zero. In both Figure 24 and Figure 25 the results can be seen when the thickest melamine foam is used(150 millimeters) and the simulations are compared to the experimental results where three aligned microphones are used as explained in subsection 5.1.3. At a later stage in this chapter the differences in thicknesses of melamine foam. Also the difference between the use of two or three microphones are shown.
Figure 24a, Figure 24b and Figure 24c show good resemblance for the absorption coefficient, as the average difference of the absorption coefficient is only 0.1. The extreme peaks that occur in the results of the experimental test setup and the simulated test setup occur (for instance at 3134 Hz in Figure 24a) , can be related to the eigenfrequency of the cavity. The extreme peaks do not occur at the same frequencies. Though these 'faults' could be related to eigenfrequencies generated by the speaker or the material specifications chosen in the simulation. Upon seeing extreme peaks in both the measurements and the simulations shows that the method can also calculate eigenfrequencies. The Figure 24d, Figure 24e and Figure 24f show some resemblance of the absorption coefficient, as the average difference of the absorption difference is 0.2 between the test setups. This remains for nearly all frequency's (except the extreme peaks).
In the graphs of the measurements of the microphones set at a maximal distance from the sound source, some resemblance can be seen between the experimental measurements and simulated measurements. As both graphs show fluctuations in the absorption coefficient between 1 and -1, the LPW method could be applicable. It is noted that the fluctuations of the absorption coefficient does not occur at the same frequency and may have differences of more then 0.5 in absorption coefficient.
Overall both Figure 24 and Figure 25 show that there is good resemblance between experiments and the simulations. However the difference between the experiments and the simulations can vary a lot, more then 0.5, in absorption coefficient.

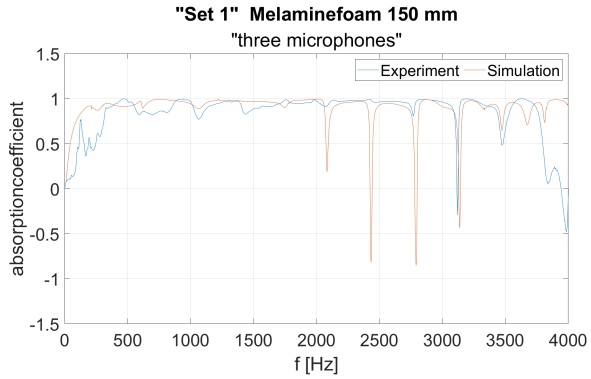

(a) Results of the absorption coefficient of microphone set 1 placed at a minimal distance to the source where melamine foam, width 150 millimeter, is added into the cavity of the experimental test setup and the simulated test setup.

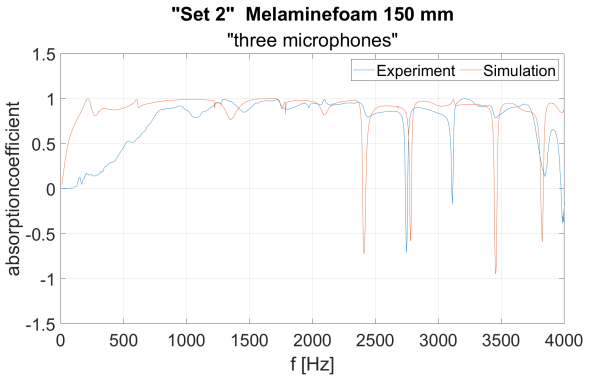

(b) Results of the absorption coefficient of microphone set 2 placed at a minimal distance to the source where melamine foam, width 150 millimeter, is added into the cavity of the experimental test setup and the simulated test setup.

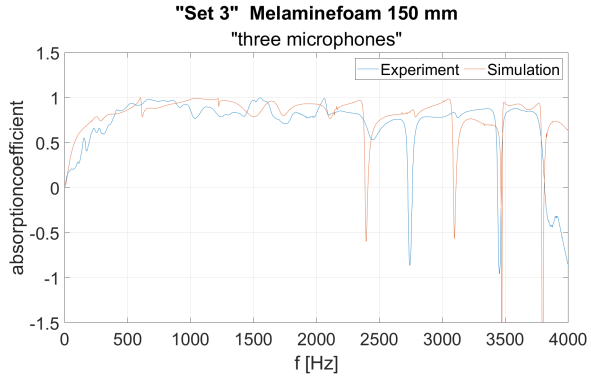

(c) Results of the absorption coefficient of microphone set 3 placed at a minimal distance to the source where melamine foam, width 150 millimeter, is added into the cavity of the experimental test setup and the simulated test setup.

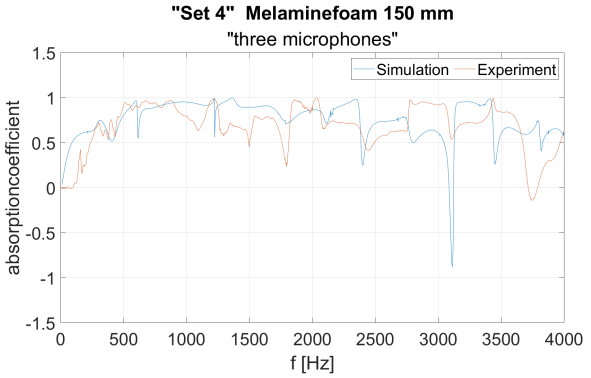

(d) Results of the absorption coefficient of microphone set 4 placed at a minimal distance to the source where melamine foam, width 150 millimeter, is added into the cavity of the experimental test setup and the simulated test setup.

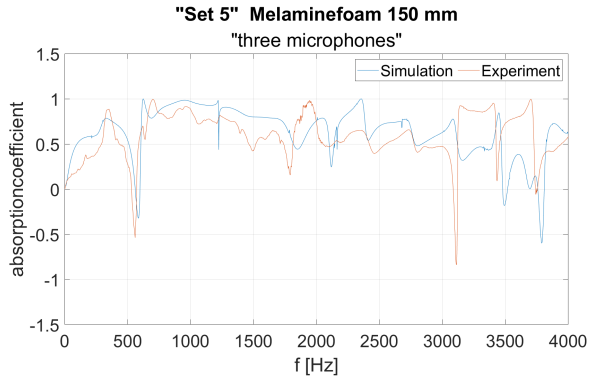

(e) Results of the absorption coefficient of microphone set 5 placed at a minimal distance to the source where melamine foam, width 150 millimeter, is added into the cavity of the experimental test setup and the simulated test setup.

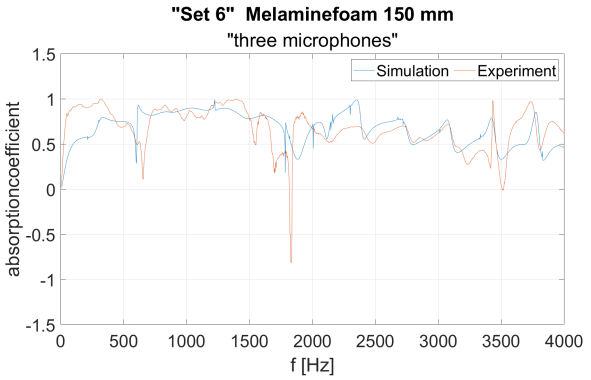

(f) Results of the absorption coefficient of microphone set 6 placed at a minimal distance to the source where melamine foam, width 150 millimeter, is added into the cavity of the experimental test setup and the simulated test setup.

Figure 24: Absorption coefficient measured vs simulation along the six microphone sets at a minimal distance to the sound source with 150 millimeter melamine foam placed in the cavity.

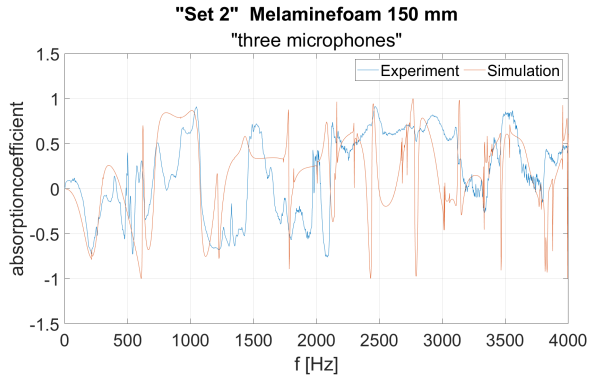

(a) Results of the absorption coefficient of microphone set 1 placed at a maximal distance to the source where melamine foam, width 150 millimeter, is added into the cavity of the experimental test setup and the simulated test setup.

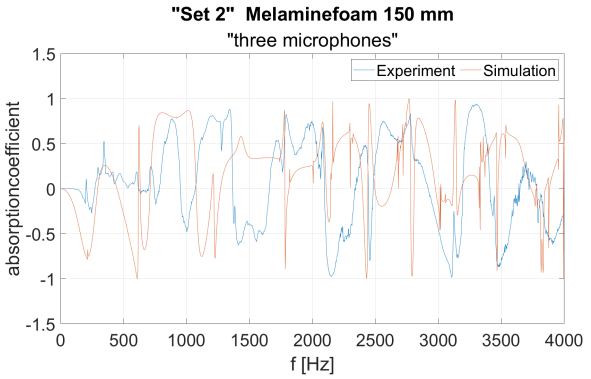

(b) Results of the absorption coefficient of microphone set 2 placed at a maximal distance to the source where melamine foam, width 150 millimeter, is added into the cavity of the experimental test setup and the simulated test setup.

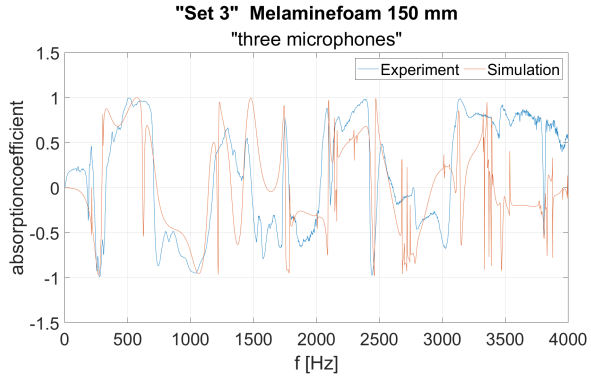

(c) Results of the absorption coefficient of microphone set 3 placed at a maximal distance to the source where melamine foam, width 150 millimeter, is added into the cavity of the experimental test setup and the simulated test setup.

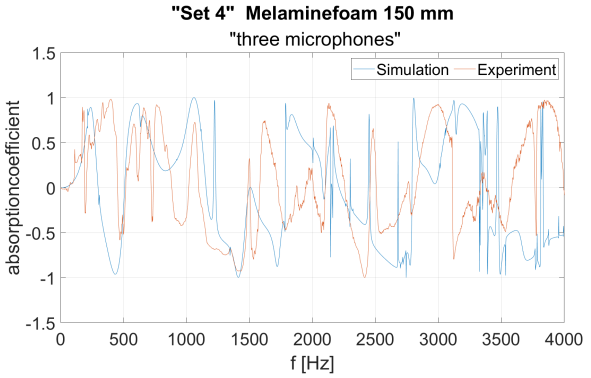

(d) Results of the absorption coefficient of microphone set 4 placed at a maximal distance to the source where melamine foam, width 150 millimeter, is added into the cavity of the experimental test setup and the simulated test setup.

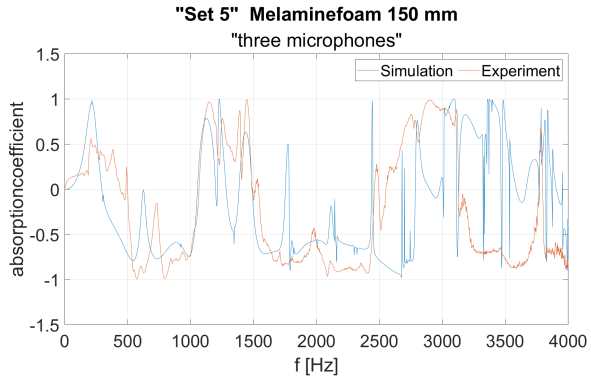

(e) Results of the absorption coefficient of microphone set 5 placed at a maximal distance to the source where melamine foam, width 150 millimeter, is added into the cavity of the experimental test setup and the simulated test setup.

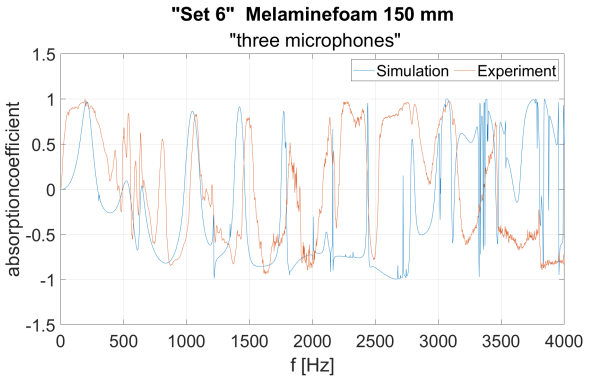

(f) Results of the absorption coefficient of microphone set 6 placed at a maximal distance to the source where melamine foam, width 150 millimeter, is added into the cavity of the experimental test setup and the simulated test setup.

Figure 25: Absorption coefficient measured vs simulation along the six microphone sets at a maximal distance to the sound source with 150mm melamine foam placed in the cavity.

6.2.1 Difference between the method with two and three microphones

In section 4, the methods are described to approximate the particle velocity. One method uses two microphones, the other, more accurate, method uses three microphones. With this approximated particle velocity, the absorption coefficient can be calculated(also given in section 4). The measurements of the six microphone sets, which are placed near the speaker, are evaluated when 150 millimeter melamine foam is added into the cavity. In Figure 26 the results of these six microphone sets are shown both the methods. In Figure 26a the results shown are quite similar, especially between 1500-2500 Hz the results are nearly the same.In the lower frequencies (<1250Hz) and in the higher frequencies, between 2750-4000 Hz, the results of the absorption coefficient differ by about 0.1.
In Figure 26b the results are almost identical up to 2000 Hz. Between 2000 Hz - 4000 Hz the magnitude of the absorption coefficient differs.
In Figure 26c, till 1250 Hz, the results show some discrepancies in the magnitude of the absorption coefficient. Between 1250 HZ and 2400 Hz the results are almost identical, between 2400 Hz and 4000 Hz the results show more discrepancies however. The eigenfrequencies are also occuring at the same frequencies, which is also the case in Figure 26a and Figure 26b.
In Figure 26d till 1700 Hz the results show discrepancies, only between 900 Hz - 1100 Hz and 1300 Hz - 1550 Hz the results are similar. Between 1700 Hz and 2700 Hz the results are quite identical, and from 2700 Hz - 4000 Hz the discrepancies will show up. What is interesting is that these results show no eigenfrequencies.
In Figure 26e discrepancies are shown across the whole domain between 0 Hz -4000 Hz, with the exception of a frequency range between 1000 Hz - 1500 Hz , 1750 Hz - 2000 Hz. The results of the eigenfrequencies are also identical.
In Figure 26f till 950 Hz discrepancies are seen between the results. In the frequency domain between 950 Hz - 3400 Hz the results are almost identical and in the frequencies between 3400 Hz - 4000 Hz discrepancies are noted.
So overall, except for the second microphone set, it can be seen that in the lower frequency range (<750Hz) the discrepancies between the results of using the method of two and the method using three microphones are significant(>0.2). In the frequencies higher than 750 Hz however, the results of the absorption coefficient become (more)identical. This could mainly be caused by the larger wave length at the lower frequencies then the wave length at the higher frequencies. As the microphones are placed close to each other, (longer)waves at lower frequency are harder to measure. Other discrepancies are seen when the eigenfrequencies occur.

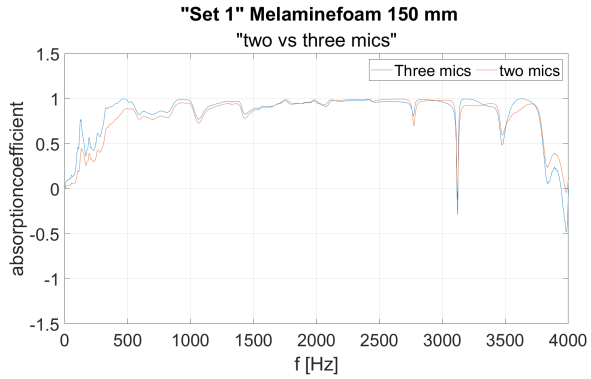

(a) Results of microphone Set 1 placed at a minimal distance to the source where melamine foam, width 150 millimeter, is added into the cavity at x=200.
Results show the difference between the method with two microphones and the method with three microphones.

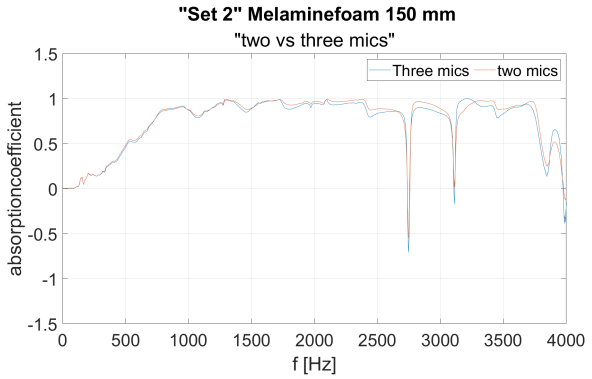

(b) Results of microphone Set 2 placed at a minimal distance to the source where melamine foam, width 150 millimeter, is added into the cavity at x=200.
Results show the difference between the method with two microphones and the method with three microphones.

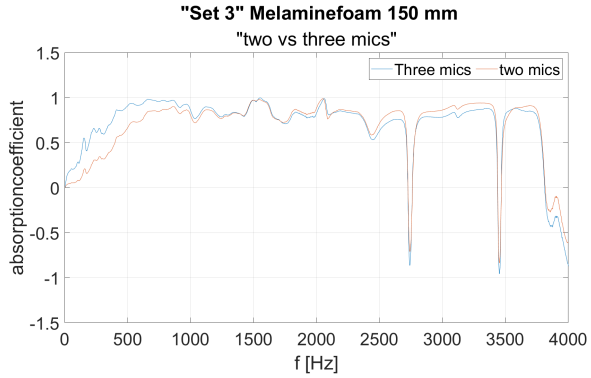

(c) Results of microphone Set 3 placed at a minimal distance to the source where melamine foam, width 150 millimeter, is added into the cavity at x=200.
Results show the difference between the method with two microphones and the method with three microphones.

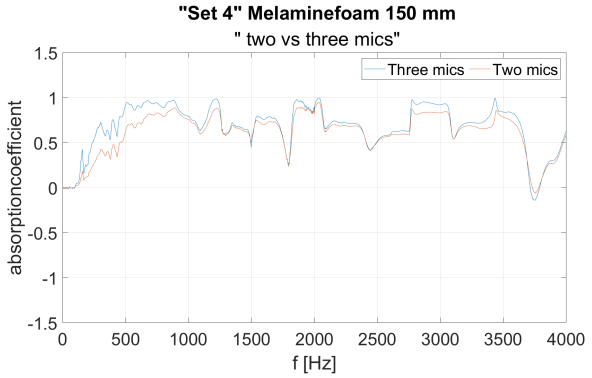

(d) Results of microphone Set 4 placed at a minimal distance to the source where melamine foam, width 150 millimeter, is added into the cavity at x=200.
Results show the difference between the method with two microphones and the method with three microphones.

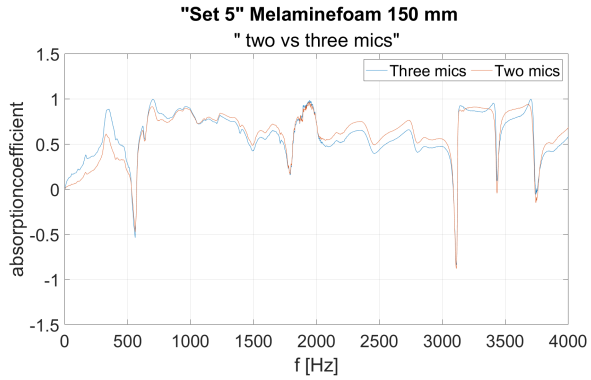

(e) Results of microphone Set 5 placed at a minimal distance to the source where melamine foam, width 150 millimeter, is added into the cavity at x=200.
Results show the difference between the method with two microphones and the method with three microphones.

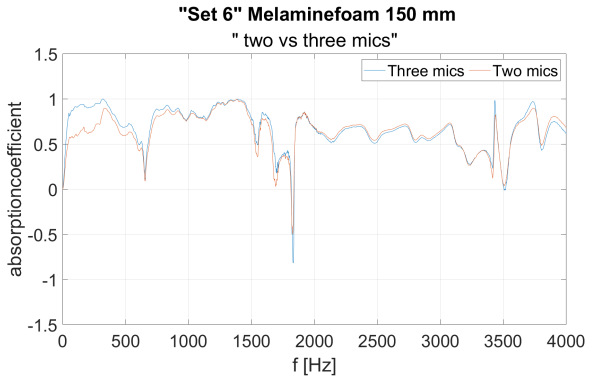

(f) Results of microphone Set 6 placed at a minimal distance to the source where melamine foam, width 150 millimeter, is added into the cavity at x=200.
Results show the difference between the method with two microphones and the method with three microphones.

Figure 26: Results of the six microphone sets placed at a minimal distance to the source where melamine foam, width 150 millimeter, is added into the cavity at x=200.
Results show the difference between the method with two microphones and the method with three microphones.

6.2.2 Variation in thickness

For the analysis of the melamine foam, the merged results of all the six microphone sets at different thicknesses of melamine foam are be discussed, to know the effect on the absorption coefficient. The melamine foam is a good absorber. So it can be expected that in the cavity is a high absorption coefficient. To check one measures the effect of the thickness on the absorption coefficient, melamine foam is placed in the cavity where thicknesses across the width are altered. The height and length of the melamine foam are set to 40 millimeter and 500 millimeter for each of the altered thicknesses. Measurements can be done between x2=167 and x1=400, so the maximum thickness in the width to place inside the cavity is 150 millimeter in order for the microphones to measure the absorption coefficient in front the material(x=167) and behind the material(x=400). As the close spaced microphones need about 75 millimeter in width. To evaluate the influence of the thicknesses various thicknesses of 50,100 and 150 millimeter have been chosen. In Figure 27, the merged results of all the six microphone sets with different thicknesses can be seen where the microphones are placed in front of the melamine foam(x2=167).

The test setup is a closed box, so the merged calculations of the absorption coefficient for microphones set 1 to microphone set 6 for an empty cavity should be zero for all frequency's. When reviewing the results regarding an empty cavity, Figure 27d, it can be said that the absorption coefficient for an empty cavity is fluctuating between 0.5 en -0.5 so an exact zero is not achieved. This difference might be cause as the particle velocity is approximated. The values in the particle velocity differ from -10^5 to 10^5 [m/s] when looking at the results in MATLAB. Therefore it is important to realize a very precise approximation. It is however also questionable if these fluctuations are also visible if they are set to octave bands.
An increase in amount of melamine foam into the cavity should mean a rise of the overall absorption coefficient by mean of the calculations of the microphone sets placed at x2 = 167 (in front of the melamine foam). In Figure 27c the merged results of the absorption coefficient can be seen when the melamine foam has a thickness of 50 millimeters. There it can be seen that the absorption coefficient is positive in the whole frequency domain and only fluctuations occur in the value of the absorption coefficient are seen which increase at higher frequencies. At the frequencies where the absorption coefficient is dropping below 0.8 in value, it is expected that the eigenfrequencies occur, except in the lower frequencies.
An increase in thickness should result in a higher absorption coefficient at the lower frequencies. However if looked at Figure 27b, it can be seen that when adding 50 millimeter of melamine foam more in thickness would only result in an absorption coefficient that shows less 'big dips' in the frequency domain. Also in Figure 27a little to no differences in absorption coefficient can be seen between the results of the melamine foam with a thickness of 100 millimeter and melamine foam with a thickness of 150 millimeters. Only the 'bigs dips' would decrease. This means that adding melamine foam with a thickness of more then 100 millimeters into the cavity would almost not result in a higher absorption coefficient.

So overall it can be concluded that when melamine foam is placed into the cavity, the resulting absorption coefficient near the speaker is higher than 0 which means only absorption occurs, which is expected. It can also be seen that in the low frequency domain (0-1000 Hz) the absorption coefficient is lower than in the higher frequencies. Adding more melamine foam into the cavity would give a more constant absorption coefficient, and the eigenfrequencies become less visible. It is however strange that no higher absorption coefficient can be seen at the lower frequencies.

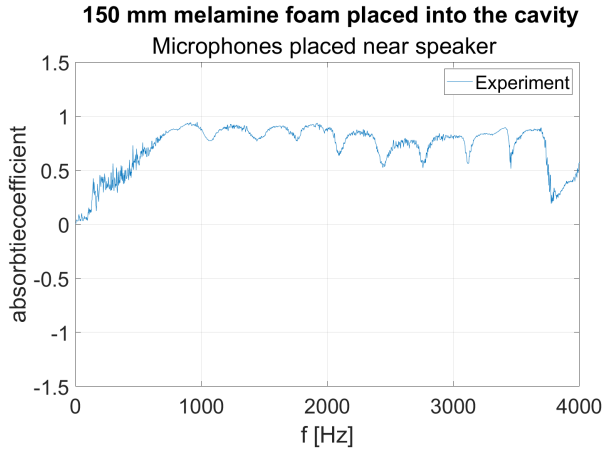

(a) Results of the absorption coefficient for all microphone sets placed at a minimal distance to the source. Within the frequency domain of 0-4000 Hz when melamine foam with a width(thickness) of 150 millimeters is placed into the test setup. Values are measured on the side of the speaker.

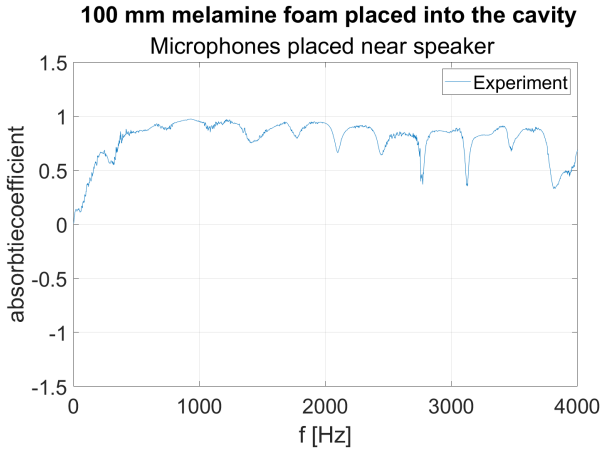

(b) Results of absorption coefficient with the microphone sets placed at a minimal distance to the source. Within the frequency domain of 0-4000 Hz when melamine foam with a width(thickness) of 100 millimeters is placed into the test setup. Values are measured on the side of the speaker.

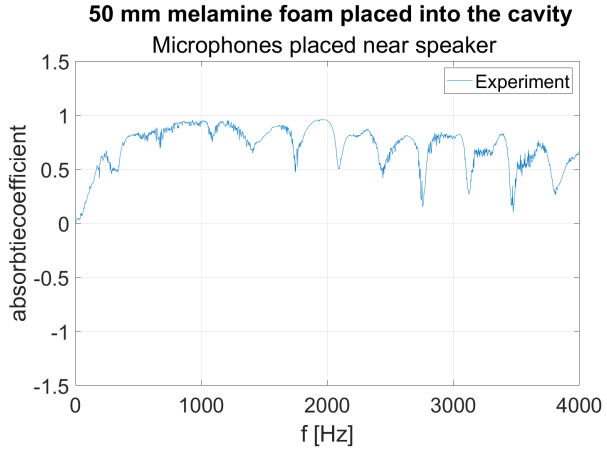

(c) Results of the absorption coefficient with the microphone sets placed at a minimal distance to the source. Within the frequency domain of 0-4000 Hz when melamine foam with a width(thickness) of 50 millimeters is placed into the test setup. Values are measured on the side of the speaker.

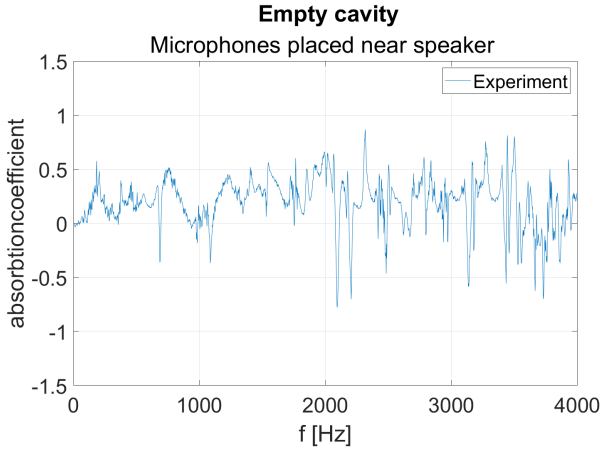

(d) Results of the absorption coefficient with the microphone sets placed at a minimal distance to the source.
Within the frequency domain of 0-4000 Hz and is placed into an empty test setup. Values are measured on the side of the speaker.

Figure 27: Total absorption coefficient spectrum with different sizes of melamine foam placed into the cavity of the experimental test setup. Values are measured on the side of the speaker.

6.3 Eigenfrequency analyses

In the section 6.2.2 it is shown that the absorption coefficient differs a lot when the eigenfrequencies occur. At least that is expected, therefore an analyses is done to review when the eigenfrequencies occur and if the big dips can be referred to the eigenfrequencies.

In COMSOL the feature 'Eigenfrequency analyses' calculates and shows the eigenfrequencies that are happening for a given domain for a simulation. This feature is used to determine the eigenfrequencies for the test setup. When looking at the eigenfrequencies one eigenfrequency, which is reoccurring each around 340Hz, is expected to explain the dips. As an example, in Figure 28, the behaviour of this eigenfrequency is shown at 2783 Hz.

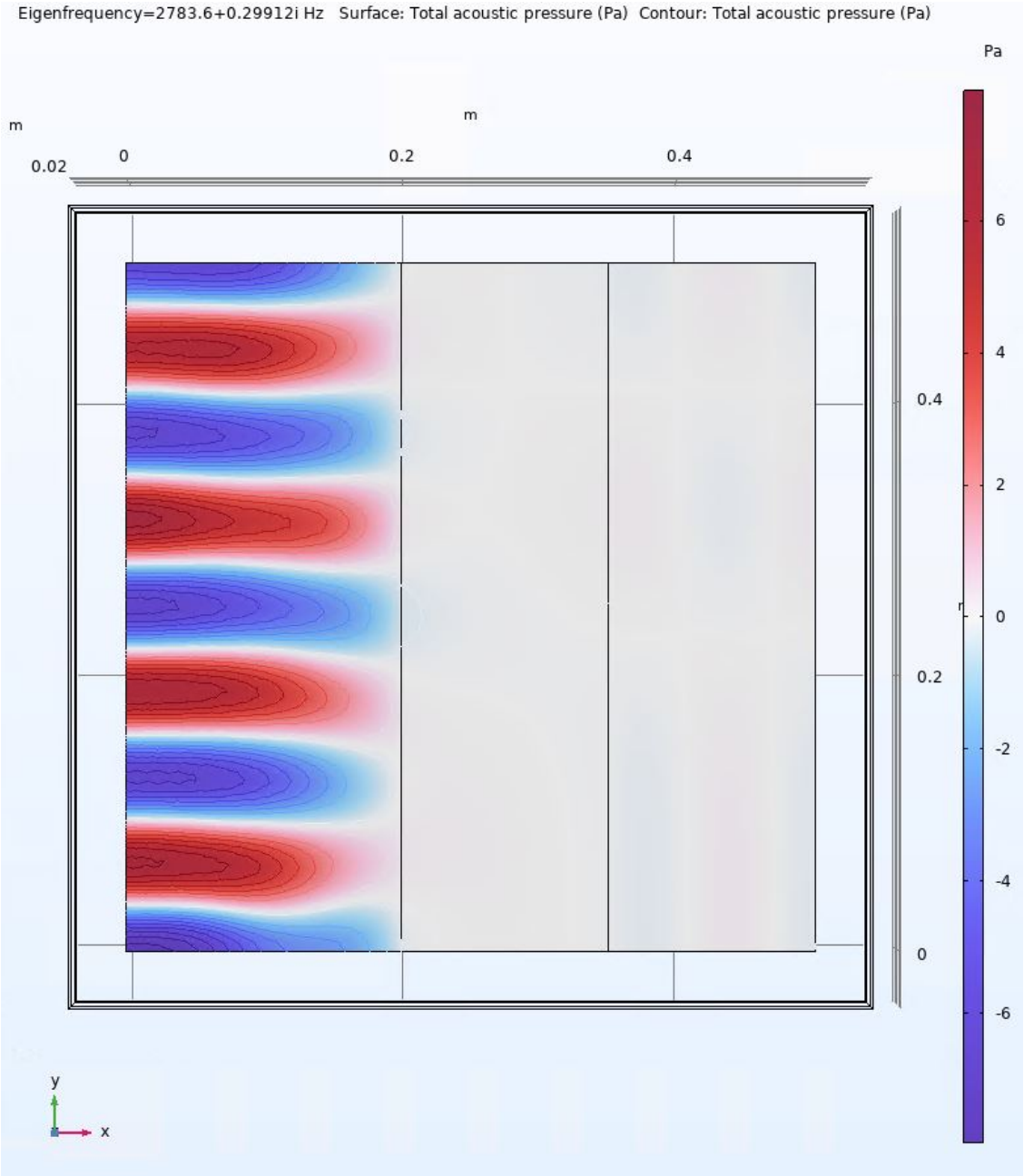

Figure 28: Top view of simulation showing the behaviour of the eigenfrequency at 2783 Hz

There is also investigated if these 'big dips' would occur in the simulation. In Figure 29 the absorption coefficient can be seen for the test setup with 50mm melamine foam. As expected the big dips are also appearing in the simulation and the eigenfrequencies are occurring at the place of the dips.

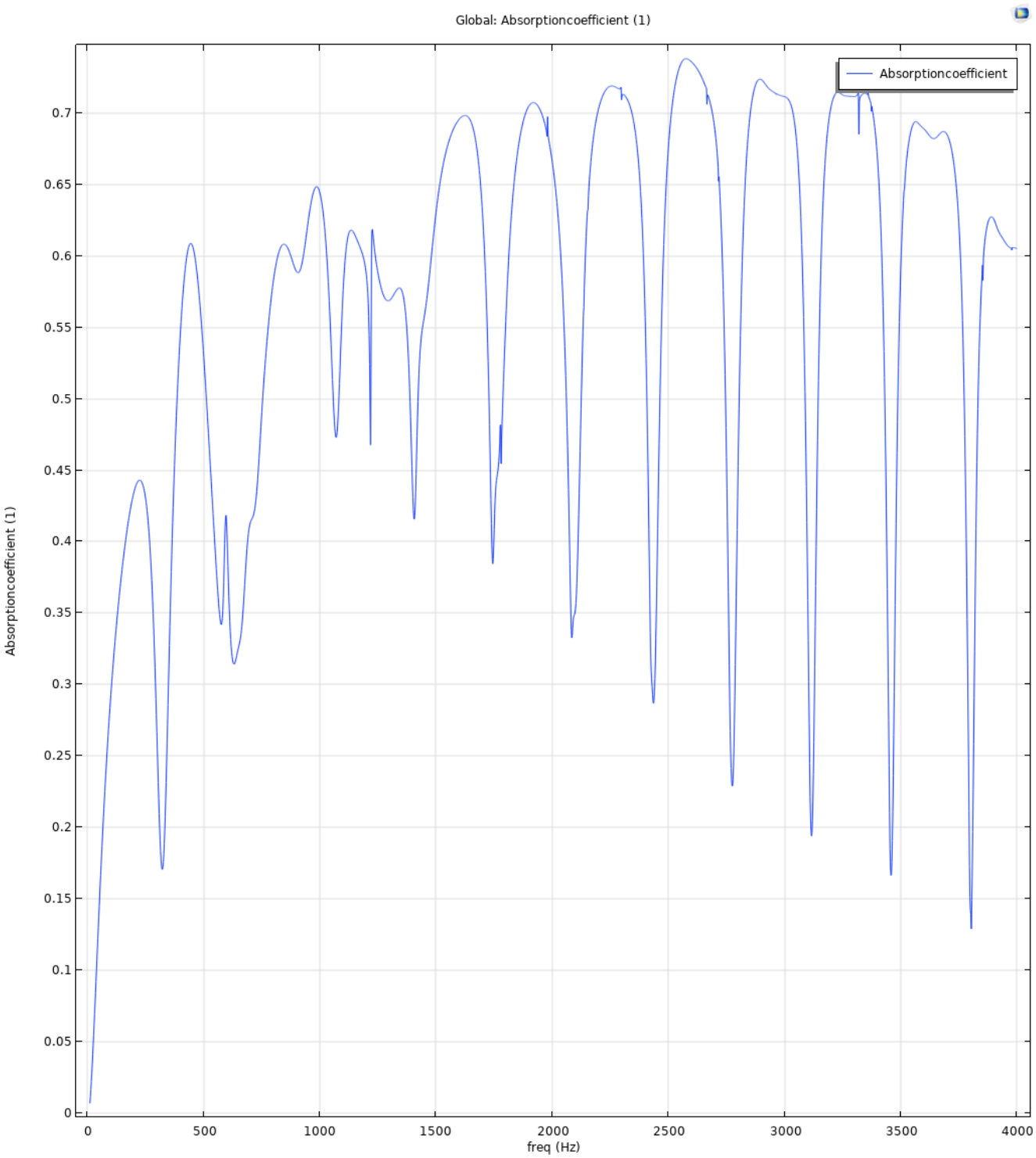

Figure 29: The merged absorption coefficient results of the six microphones in front of 50 millimeter melamine foam

In section 6.2.2 it is shown that in the experiments the big dips decrease when thicker foam is placed in the test setup. Figure 30 show the results of the simulated merged absorption coefficient when the foam is 150 millimeter thick. Unfortunately, the decrease in the 'big dips' can not be seen.

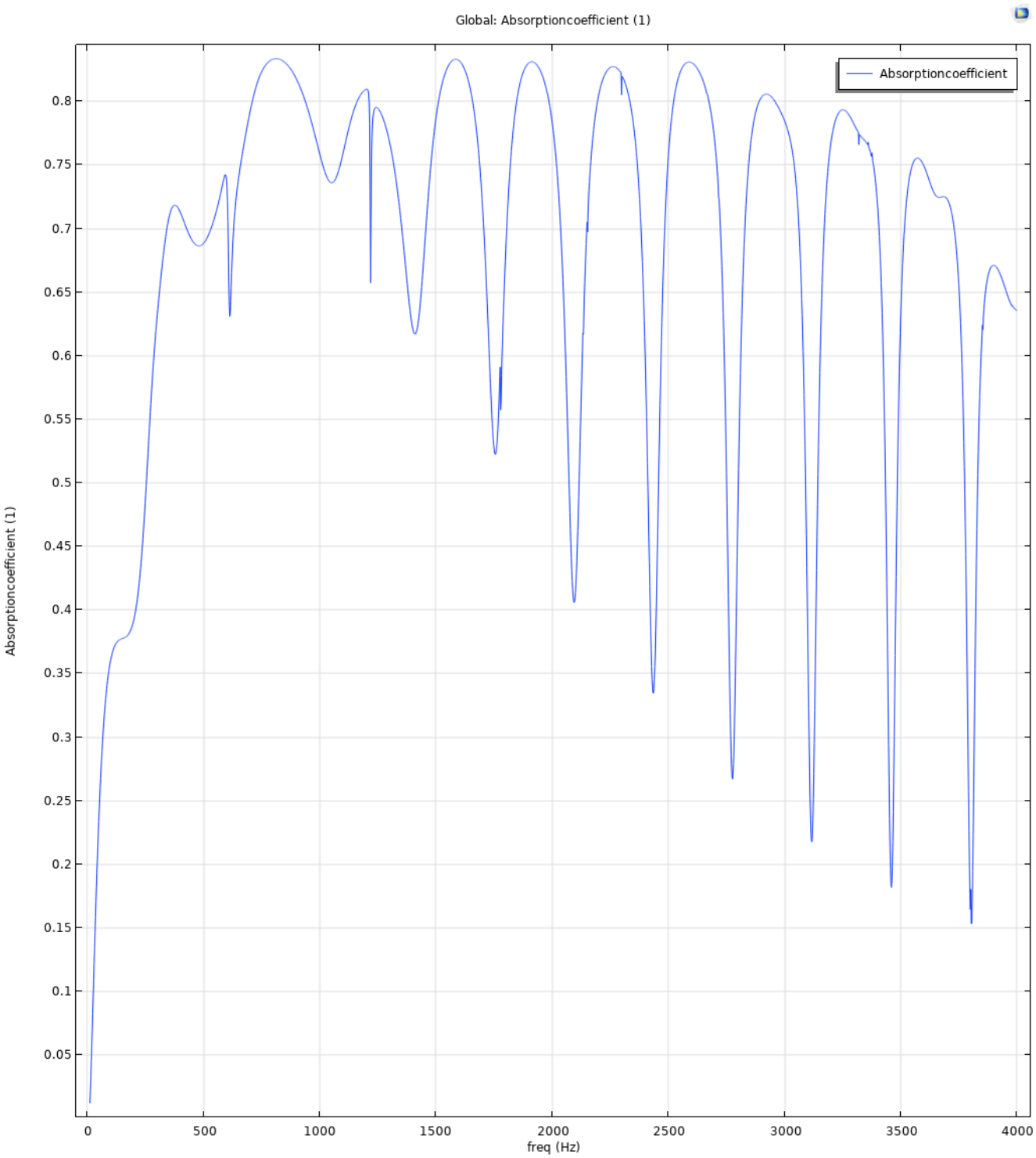

Figure 30: The merged absorption coefficient results of the six microphones in front of 150 millimeter melamine foam

7 Conclusion & Discussion

7.1 Conclusion

One can conclude that the box can be used to experimentally validate the plane wave decomposition (PWD), as initial measurements based on the slightly simpler local plane wave (LPW) method could be validated easily. The results show that the measured absorption coefficient is in line with the numerical model. More research is needed to also align the measured sound pressure level and particle velocity levels to the values obtained in the numerical model. The derivation of the particle velocity based on the 3 microphone method is shown to be more accurate than the 2 microphone based method.

7.2 Discussion

The speaker is represented in the simulation software as a source which produces pressure. In a real situation a sound pressure source should not be represented by a speaker, as a speaker may also produces a particle velocity, vibrations and other properties which could influence the calculated results of the simulation. This could explain the simulation results of the L_p and the L_v. A better representation of the speaker may give more accurate results for representation of the pressure and velocity field.

Currently only the LPW method is applied on the experimental measurements to calculate the absorption coefficient. This is done as there was given a lot of time at gaining a relation between either, the experimental L_p and the simulated L_p or the experimental L_v or simulated L_v. Unfortunately a relation was not found. Because of this there was chosen to stop searching for a relation between the experimental measurements and the simulated measurements for validation of the L_p and L_v. It was decided to find a relation for the absorption coefficient by starting with only the LPW method as this is the main purpose of this paper. As shown a relation was found. By applying the LPW method less mistakes can be made in the formula when implementing it in MATLAB. In further research a more in depth method could be applied(LSPW or LAPW) and further development of numerical equation of the incident intensity in equation 36 can be established.
In an empty cavity the absorption coefficient should be 0 for all frequencies if the sum of all 6 microphones sets are integrated. However in the Figure 27 a lot of fluctuations can be seen around 0 in an empty cavity. These fluctuations could attribute to the importance of more accurately approximating the particle velocity.

References

[1] R.P.Bontekoning, *The plane wave decomposition of the solutions of the Helmholtz equation.* University of Twente, 2022.

[2] Y. H. Wijnant, E. Kuipers, and A. de Boer, *Development and application of a new method for the in-situ measurement of sound absorption*, 2010, vol. 31.

[3] E. R. Kuipers, *Measuring sound absorption using local field assumptions.* University of Twente Enschede, The Netherlands, 2013.

[4] Y. H. Wijnant, "On the local plane wave methods for in situ measurement of acoustic absorption," in *21st International Congress on Sound and Vibration, ICSV 2014*. International Institute of Acoustics and Vibration (IIAV), 2015.

[5] Y. Wijnant, *Notes Engineering Acoustics.* University of Twente, Faculty of Engineering Techology, 2023.

[6] V. Germany, "Visaton bf 32 - 8 ohm," Visaton GmbH, Tech. Rep., 2023.

[7] G. S. . Vibration, "Gras 40ph-10 ccp free-field array microphone," 2024. [Online]. Available: https://www.grasacoustics.com/products/special-microphone/array-microphones/product/830-gras-40ph-10-ccp-free-field-array-microphone

[8] N. I. Corp., "Pxie-1073 specifications," 2024, last updated 8 August 2023. [Online]. Available: https://www.ni.com/docs/en-US/bundle/pxie-1073-specs/page/specs.html

[9] G. . Acociates, "Acoustic glossery," 2024, last accessed 2 Januari 2024. [Online]. Available: https://www.acoustic-glossary.co.uk/definitions-r.htm#reference

Nomenclature

Symbols

$\Im$	Imaginary part
$\Re$	Real part
ρ	Density
A	Complex amplitude A wave
B	Complex amplitude B wave
c	Speed of sound
f	Frequency
I_{ac}	Active sound intensity
I_{in}	Incident sound intensity
I_{refl}	Reflected sound intensity
k	Wave number
L_p	Sound pressure level
L_v	Velocity level
P	Complex pressure
p_{ref}	Reference pressure
p_{rms}	Root mean square pressure
v_{ref}	Reference velocity
v_{rms}	Root mean square velocity
W_{ac}	Active sound power
W_{in}	Incident sound power
Z	Impedance

Greek Symbols

α	Absorption coefficient/ Angle of A wave with the x axis
β	Angle of B wave with the x axis
λ	Wave length
ω	Angular frequency
$\theta_{I_{re}}$	Angle of reactive intensity with the x axis

Abbreviations

LPW	Local Plane Wave
$LSPW$	Local Specular Plane Wave
PWD	Plane Wave Decomposition

Appendix

A Drawings of the test setup

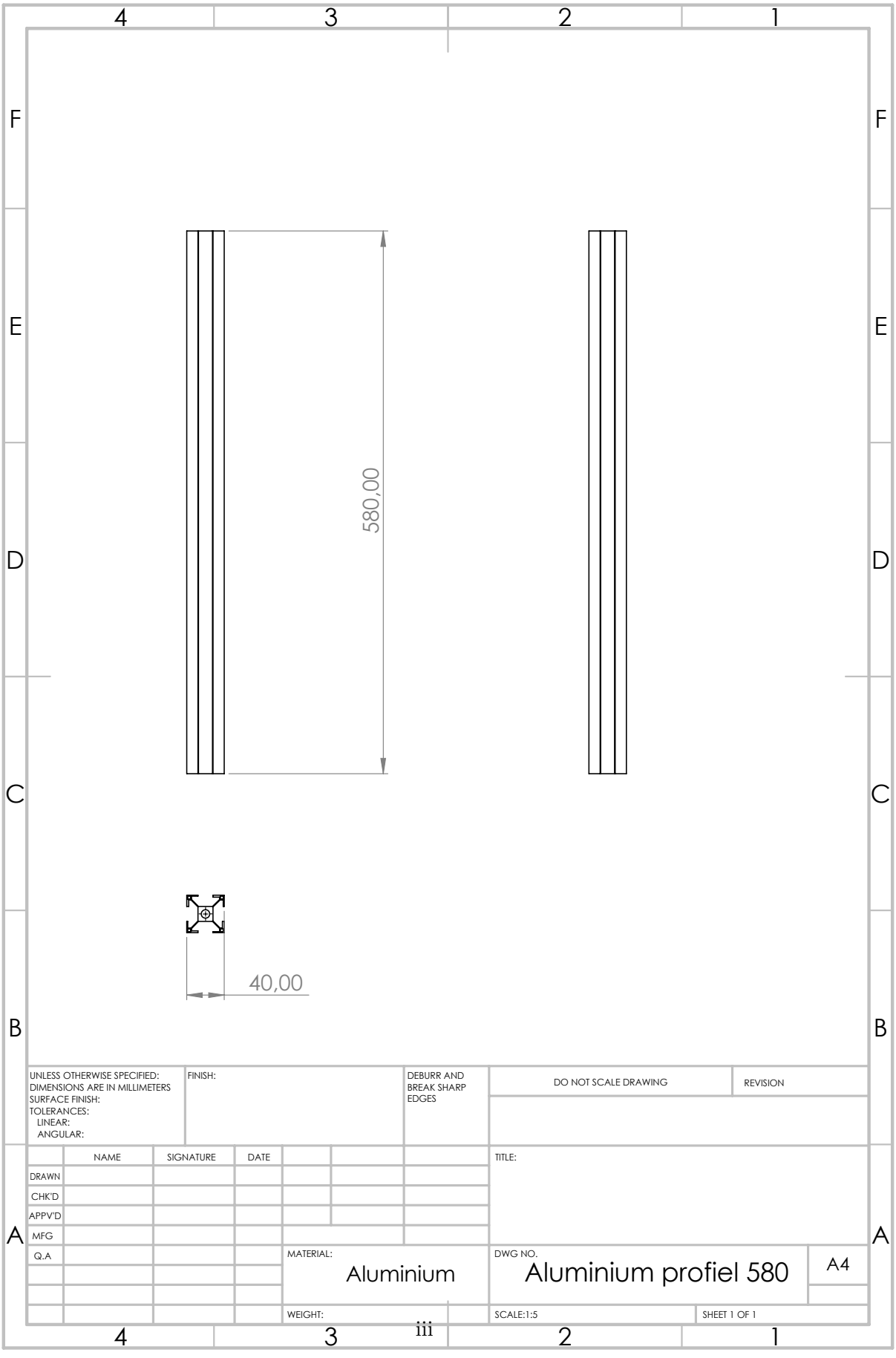

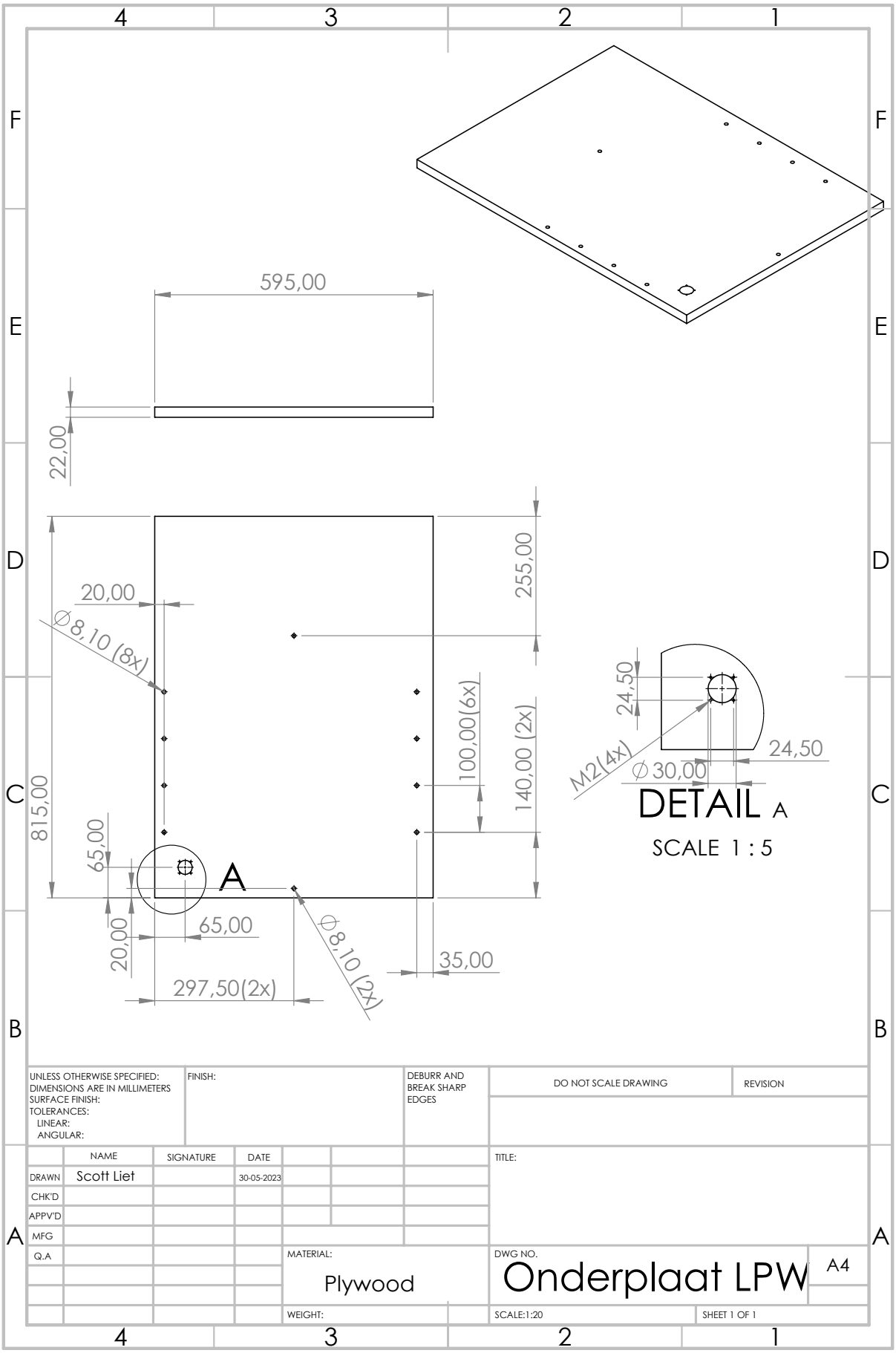

Figure 32: Dimensions wooden bottom plate

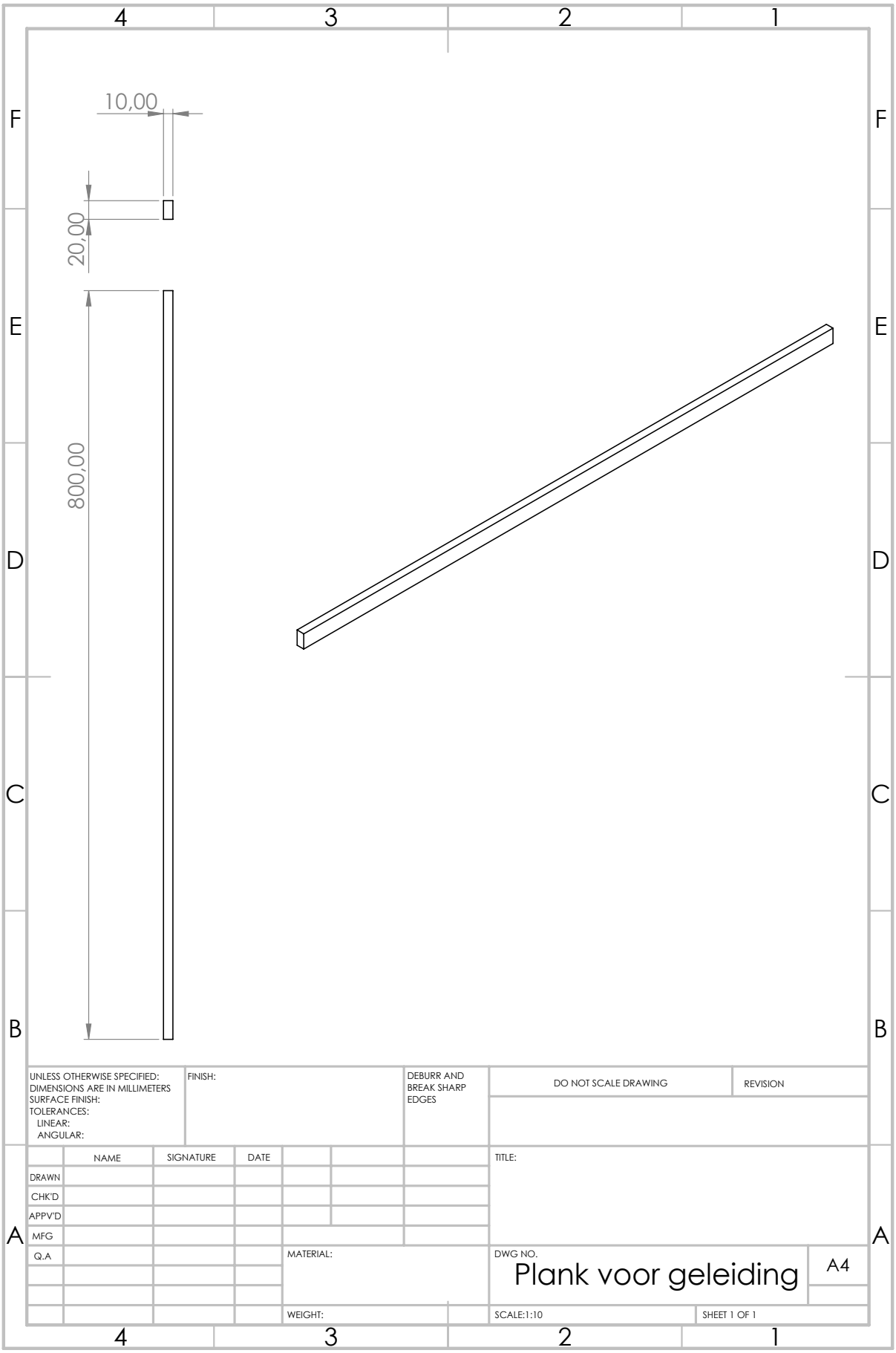

Figure 33: Dimensions gliding plank

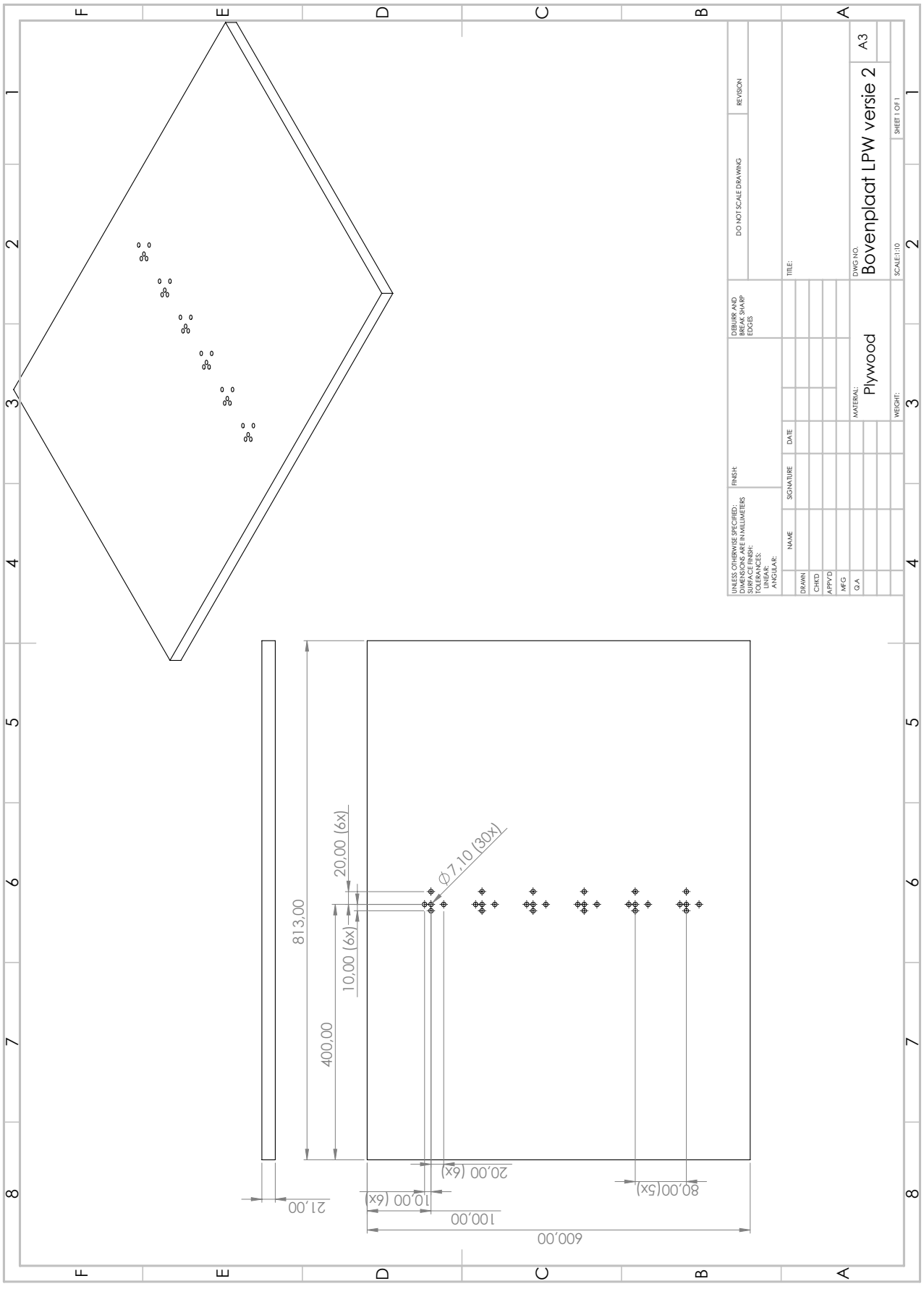

Figure 34: Dimensions wooden top plate

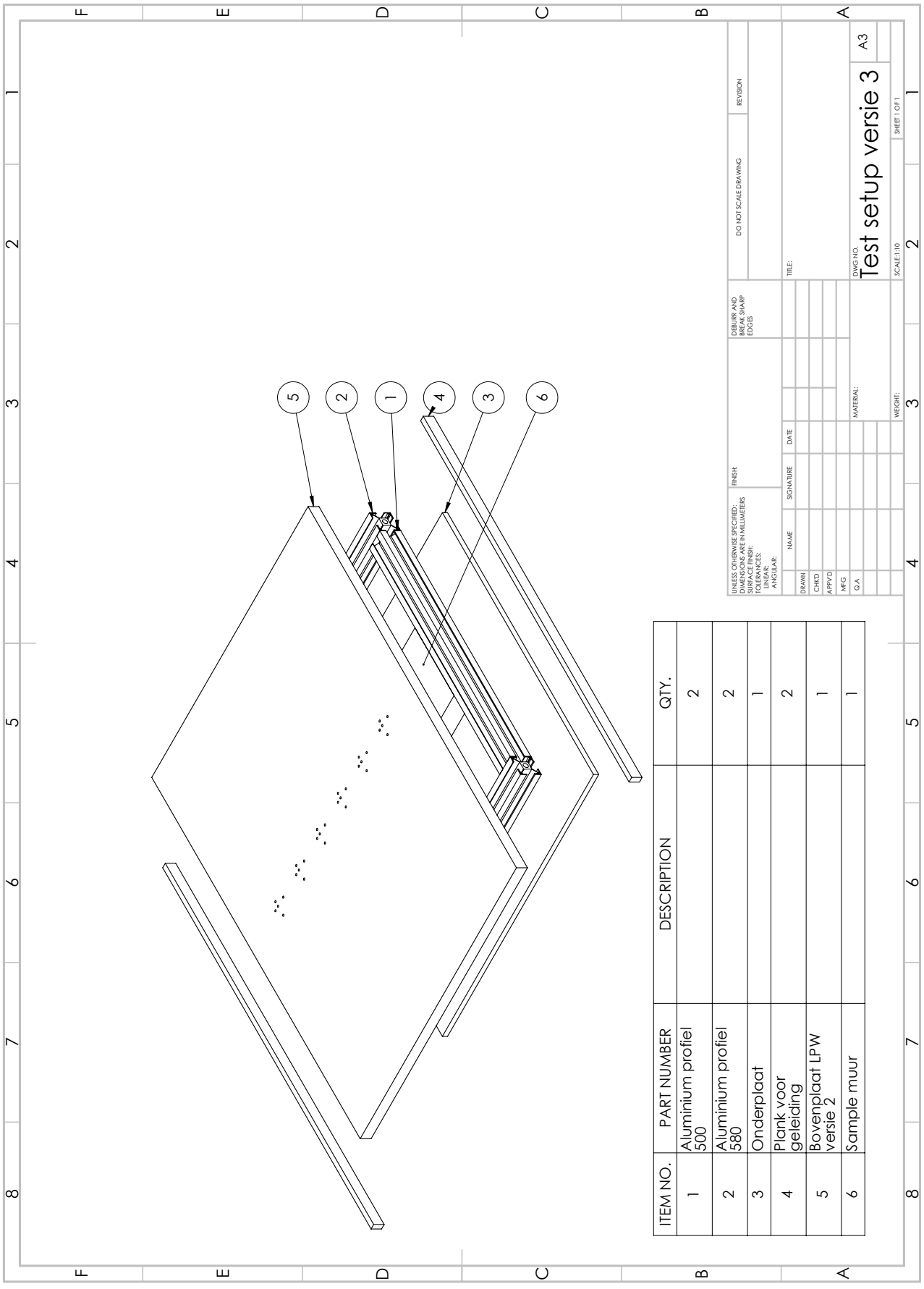

Figure 35: Total test setup

B Specifications of the speaker

GERMANY
VISATON®

BF 32
Art. No. 2243 – 4 Ω
Art. No. 2242 – 8 Ω

CAD | °C –25 +70

3,2 cm (1,3") Breitbandlautsprecher mit breitem, ausgewogenem Frequenzgang und sehr guter Tieftonwiedergabe. Mit kräftigem Neodym-Antrieb. Geeignet für Anwendungen, die zugleich geringe Abmessungen und gute Musik- und Sprachwiedergabe fordern. Quadratischer Korb mit vier Befestigungslöchern ermöglicht einfache Montage. Silberne Membran.

Anwendungsmöglichkeiten: Flachbildschirmen (TV und PC). Infoterminals. Andere kompakte Geräte und Automaten zur Sprach- und Musikwiedergabe

3.2 cm (1.3") fullrange speaker *with a wide and balanced frequency response and very good low range reproduction. With powerful Neodymium driver. Suitable for applications where slim construction and good music and speech reproduction are requested. Square basket with four mounting holes for easy mounting. Silver-coloured membrane.*

Typical applications: *flat screens (TV and PC), info terminals, other compact devices speech and music reproduction*

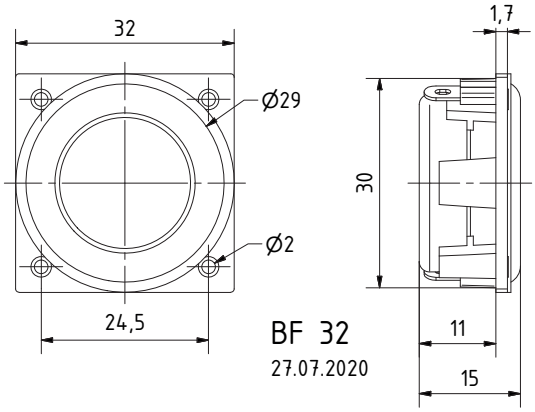

Technische Daten / *Technical Data*	
Nennbelastbarkeit *Rated power*	2 W
Musikbelastbarkeit *Maximum power*	5 W
Impedanz *Impedance*	4 Ω / 8 Ω
Übertragungsbereich (–10 dB) *Frequency response (–10 dB)*	150–20000 Hz
Mittlerer Schalldruckpegel *Mean sound pressure level*	78 dB (1 W/1 m)
Resonanzfrequenz *Resonant frequency*	280 Hz
Schwingspulendurchmesser *Voice coil diameter*	20 mm Ø
Wickelhöhe *Height of winding*	3 mm
Schallwandöffnung *Cut-out diameter*	31,5 mm Ø
Anschluss *Terminal*	Lötösen *Solder lugs*
Gewicht netto *Net weight*	28 g

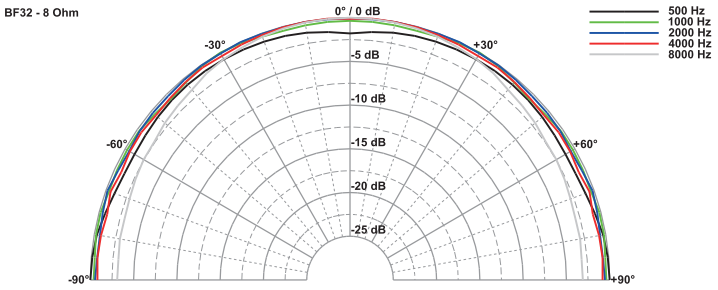

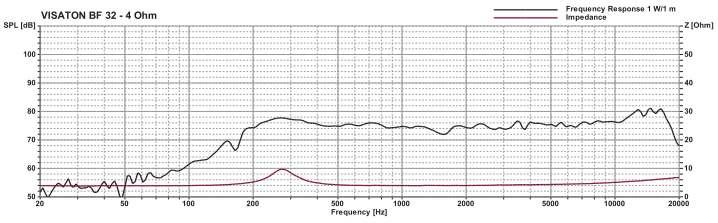

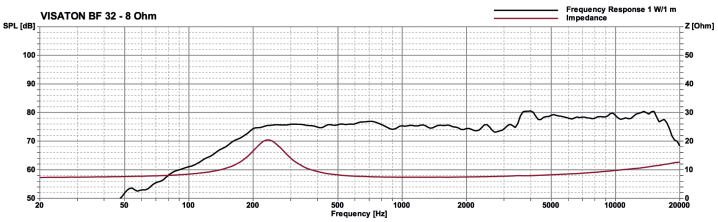

Figure 36: Specifications Visaton 32 BF [6]

C Specifications of the used microphones

Specifications

GRAS 40PH-10 CCP Free-field Array Microphone

Polarization/Connection		0 V / CCP
Frequency range (±1.5 dB)	Hz	50 to 5 k
Frequency range (±2 dB)	Hz	10 to 20 k
Dynamic range lower limit (microphone thermal noise)	dB(A)	< 33
Dynamic range upper limit	dB	135
Set sensitivity @ 250 Hz (±2 dB)	mV/Pa	50
Power supply (Constant Current Power)	mA	2 to 20
Microphone venting		Front
Output impedance	Ω	< 50
Temperature range, operation	°C / °F	-10 to 50 / -50 to 122
Temperature range, storage	°C / °F	-20 to 60 / -4 to 140
Influence of axial vibration @1 m/s²	dB re 20 µPa	55
TEDS UTID (IEEE 1451.4)		27 v. 1.0
Connector type		SMB
CE/RoHS compliant/WEEE registered		Yes / Yes / Yes
Weight	g / oz	5.50 / 0.20
Phase Match		
50Hz - 100Hz		±5°
100Hz - 3kHz		±3°
3kHz - 5kHz		±5°
5kHz - 10kHz		±10°

Frequency response according to IEC 61672-1

Figure 37: Specifications Microphones

Specifications

GRAS 40PH-10 CCP Free-field Array Microphone

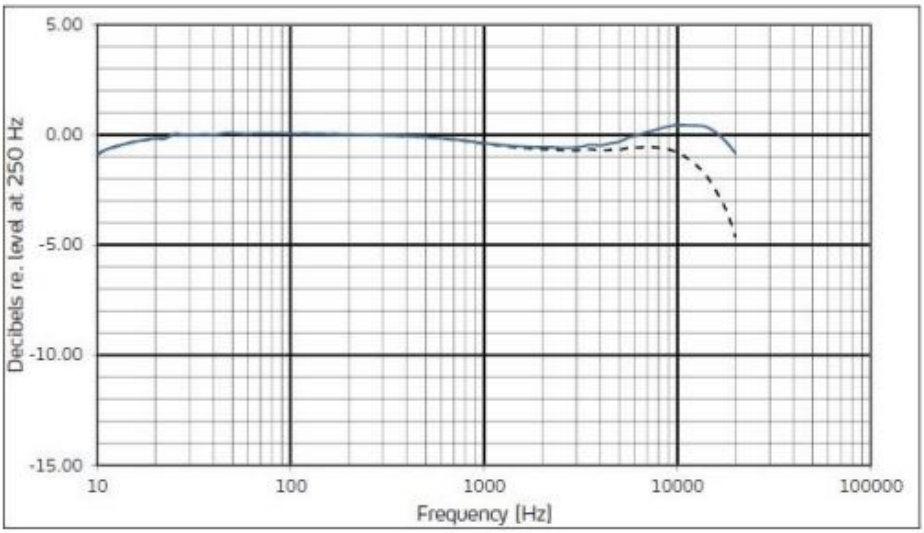

Typical frequency response

Upper curve shows free-field response at 0°, lower curve (dotted line) shows pressure response.

GRAS Sound & Vibration reserves the right to change specifications and accessories without notice.

Figure 38: Specifications Microphones

D Results of the L_p & L_v

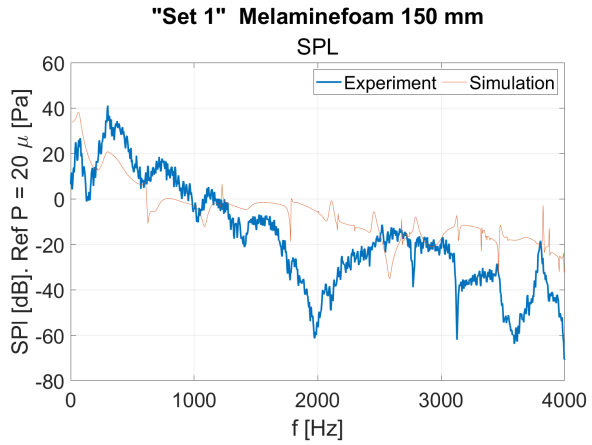

(a) L_P:Results of the L_p of microphone set 1 placed at a minimal distance to the source where melamine foam, width 150 millimeter, is added into the cavity of the experimental test setup and the simulated test setup.

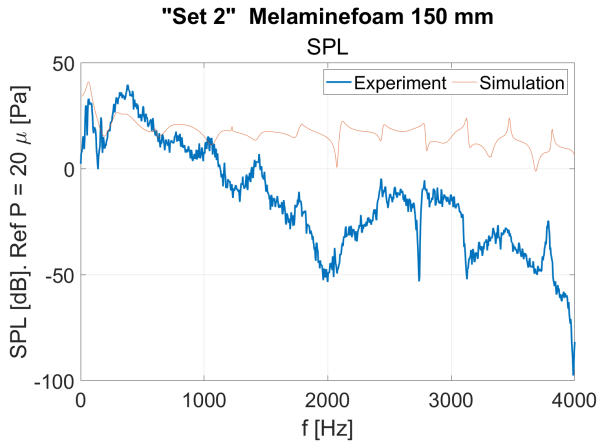

(b) L_P: Results of the L_p of microphone set 2 placed at a minimal distance to the source where melamine foam, width 150 millimeter, is added into the cavity of the experimental test setup and the simulated test setup.

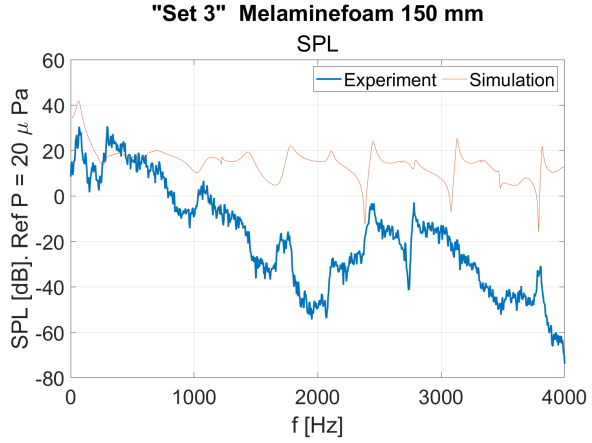

(c) L_P: Results of the L_p of microphone set 3 placed at a minimal distance to the source where melamine foam, width 150 millimeter, is added into the cavity of the experimental test setup and the simulated test setup.

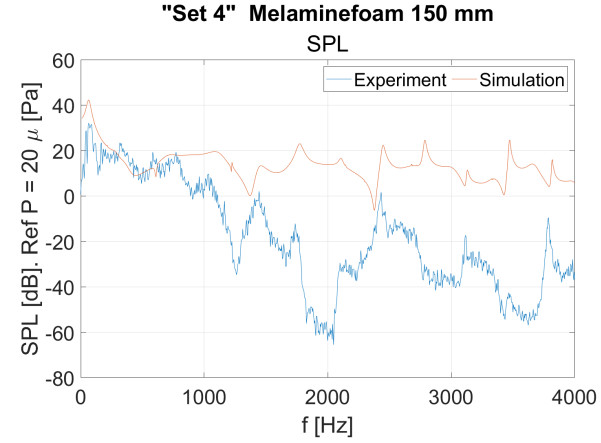

(d) L_P: Results of the L_p of microphone set 4 placed at a minimal distance to the source where melamine foam, width 150 millimeter, is added into the cavity of the experimental test setup and the simulated test setup.

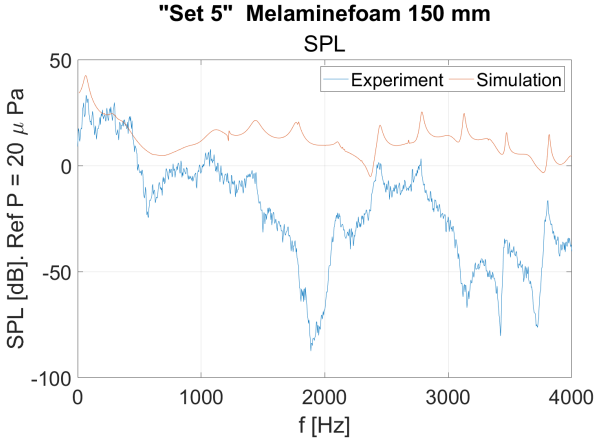

(e) L_p: Results of the L_p of microphone set 5 placed at a minimal distance to the source where melamine foam, width 150 millimeter, is added into the cavity of the experimental test setup and the simulated test setup.

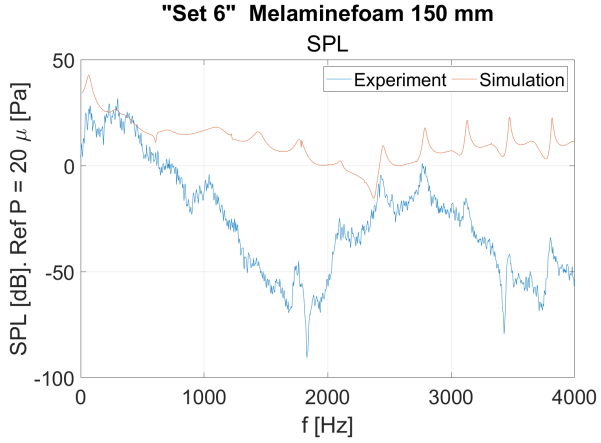

(f) L_p: Results of the L_p of microphone set 6 placed at a minimal distance to the source where melamine foam, width 150 millimeter, is added into the cavity of the experimental test setup and the simulated test setup.

Figure 39: L_P measured vs simulation along the six microphone sets at a minimal distance to the source where melamine foam, width 150 millimeter, is added into the cavity of the experimental test setup and the simulated test setup.

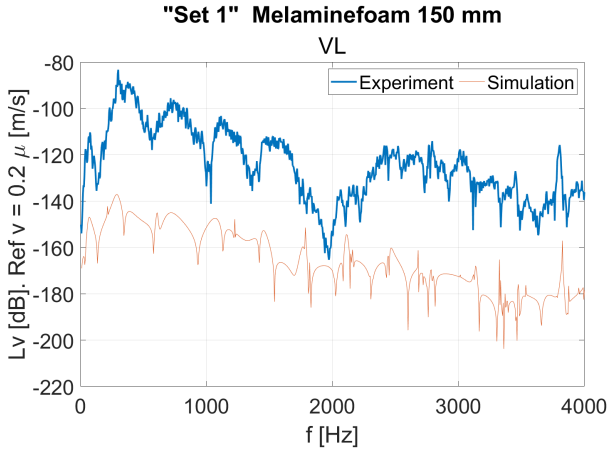

(a) L_v: Results of the L_v of microphone set 1 placed at a minimal distance to the source where melamine foam, width 150 millimeter, is added into the cavity of the experimental test setup and the simulated test setup.

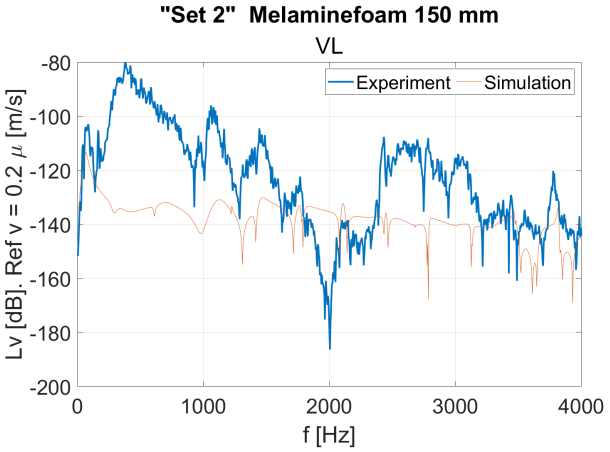

(b) L_v: Results of the L_v of microphone set 2 placed at a minimal distance to the source where melamine foam, width 150 millimeter, is added into the cavity of the experimental test setup and the simulated test setup.

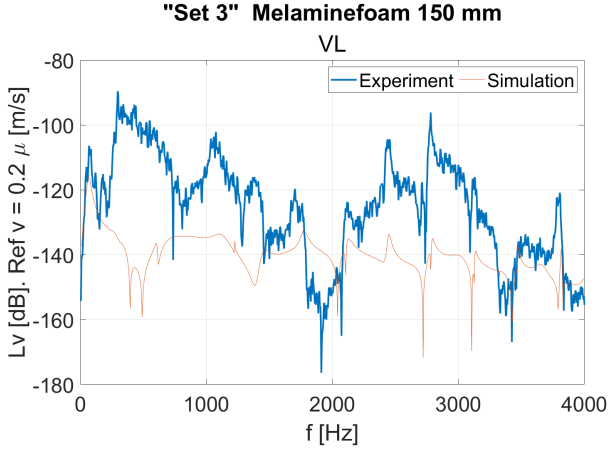

(c) L_v: Results of the L_v of microphone set 3 placed at a minimal distance to the source where melamine foam, width 150 millimeter, is added into the cavity of the experimental test setup and the simulated test setup.

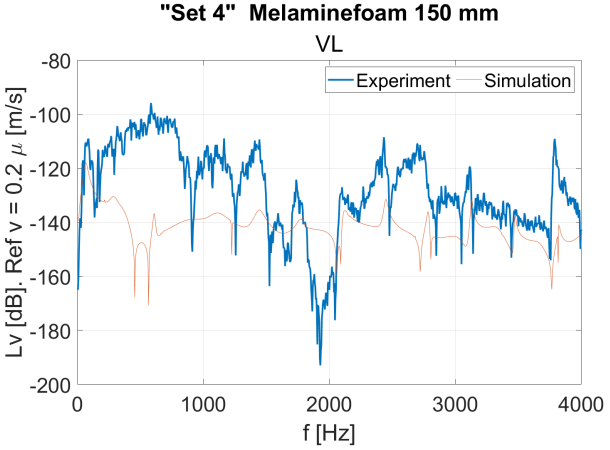

(d) L_v: Results of the L_v of microphone set 4 placed at a minimal distance to the source where melamine foam, width 150 millimeter, is added into the cavity of the experimental test setup and the simulated test setup.

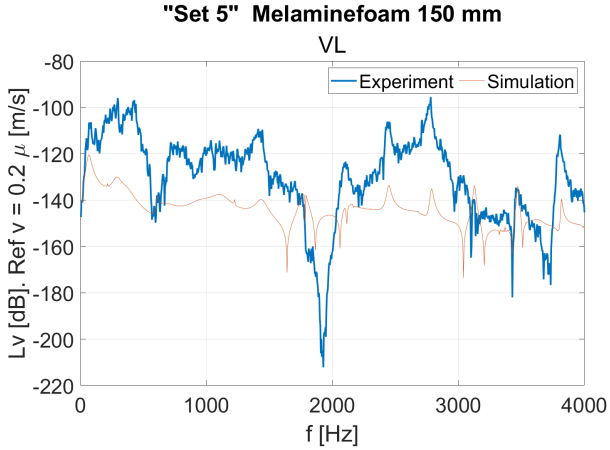

(e) L_v: Results of the L_v of microphone set 5 placed at a minimal distance to the source where melamine foam, width 150 millimeter, is added into the cavity of the experimental test setup and the simulated test setup.

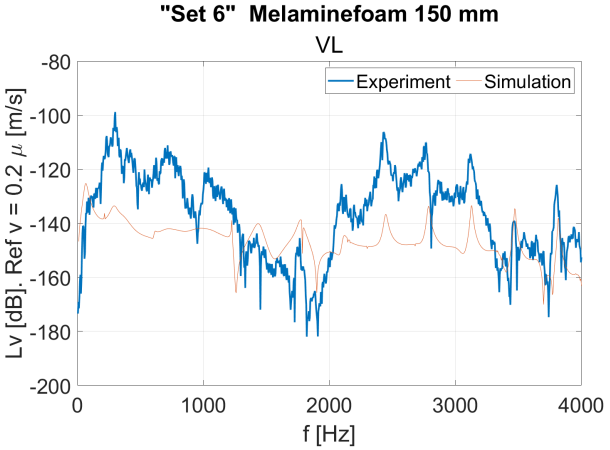

(f) L_v: Results of the L_v of microphone set 6 placed at a minimal distance to the source where melamine foam, width 150 millimeter, is added into the cavity of the experimental test setup and the simulated test setup.

Figure 40: L_v measured vs simulation along the six microphone sets at a minimal distance to the source where melamine foam, width 150 millimeter, is added into the cavity of the experimental test setup and the simulated test setup.

Acknowledgement

I would like to express my gratitude towards my supervisor, Ysbrand Wijnant, since he came up with the original ideas on which this work is largely based. His guidance and assistance throughout the process of conducting this research and writing this thesis was very valuable.
For the practical assistance received I would like to thank Walter and Elise with creating the test setup in the laboratory.